

1 **The novel *Dbl* homology/BAR domain protein, *MsgA*, of *Talaromyces***  
2 ***marneffe* regulates yeast morphogenesis during growth inside host cells**

3  
4 Harshini Weerasinghe, Hayley E. Bugeja and Alex Andrianopoulos\*

5  
6 Genetics, Genomics and Systems Biology, School of BioSciences, University of  
7 Melbourne, Victoria 3010, Australia

8  
9  
10  
11  
12  
13  
14  
15

16 **Keywords:** *Talaromyces marneffe*, *Penicillium marneffe*, macrophage infection,  
17 Rho guanine nucleotide exchange factor, yeast morphogenesis, pathogenic fungi,  
18 BAR domain.

19  
20 \*Corresponding author: Alex Andrianopoulos, Genetics, Genomics and Systems  
21 Biology, School of BioSciences, University of Melbourne, Victoria 3010, Australia.  
22 Telephone + 61 3 8344 5164. Email alex.a@unimelb.edu.au

23

24 **Abstract**

25 Microbial pathogens have evolved many strategies to evade recognition by the  
26 host immune system, including the use of phagocytic cells as a niche within  
27 which to proliferate. Dimorphic pathogenic fungi employ an induced  
28 morphogenetic transition, switching from multicellular hyphae to unicellular  
29 yeast that are more compatible with intracellular growth. A switch to  
30 mammalian host body temperature (37°C) is a key trigger for the dimorphic  
31 switch. This study describes a novel gene, *msgA*, from the dimorphic fungal  
32 pathogen *Talaromyces marneffe* that controls cell morphology in response to  
33 host cues rather than temperature. The *msgA* gene is upregulated during murine  
34 macrophage infection, and deletion results in aberrant yeast morphology solely  
35 during growth inside macrophages. MsgA contains a Dbl homology domain, and  
36 a Bin, Amphiphysin, Rvs (BAR) domain instead of a Plekstrin homology domain  
37 typically associated with guanine nucleotide exchange factors (GEFs). The BAR  
38 domain is crucial in maintaining yeast morphology and cellular localisation  
39 during infection. The data suggests that MsgA does not act as a canonical GEF  
40 during macrophage infection and identifies a temperature independent pathway  
41 in *T. marneffe* that controls intracellular yeast morphogenesis.

42

43

## 44 **Introduction**

45

46 Host defence against disease causing microbes involves actively identifying and  
47 eliminating invading pathogens. This begins with the innate immune system  
48 where host phagocytes engulf and destroy these microbes, followed by triggering  
49 of an adaptive immune response. The success of a pathogen depends on its  
50 ability to escape the host response and for some pathogens this involves residing  
51 within particular phagocytic cells of the host where they are then able grow and  
52 proliferate. An important factor facilitating this lifestyle is the capacity to adopt a  
53 growth form suitable for the spatial constraints of the intracellular environment  
54 of a host cell. For many fungal pathogens that utilise the intracellular  
55 environment of macrophages as a means of immune system avoidance,  
56 morphological plasticity is an important virulence attribute (Nemecek et al.  
57 2006; Nguyen & Sil 2008; Webster & Sil 2008; Beyhan et al. 2013; Brandhorst et  
58 al. 1999; Rooney et al. 2001). This is exemplified by the dimorphic fungi, which  
59 display saprophytic, multicellular, filamentous hyphal growth in the external  
60 environment and are able to adopt a unicellular yeast growth form during  
61 infection. Dysregulation of morphology, leading to the production of a growth  
62 form that disrupts the integrity of the phagocytic cells, exposes the pathogen to  
63 the entire immune system.

64

65 *Talaromyces marneffeii* (formerly *Penicillium marneffeii*) is an intracellular human  
66 pathogen that exhibits temperature dependent dimorphic growth. At 25°C it  
67 grows in a multinucleate septate hyphal form that can differentiate to produce  
68 uninucleate asexual spores (conidia) (Andrianopoulos 2002). At 37°C *in vitro* it  
69 grows as uninucleate yeast that divides by fission. The transition from hyphal  
70 cell or dormant conidium to a yeast cells proceeds by arthroconidiation, a  
71 process of filament fragmentation, in which nuclear and cellular division are  
72 coupled, double septa are laid down with subsequent cell separation producing  
73 yeast cells (Andrianopoulos 2002). The transition from yeast cell to hyphal cell  
74 occurs by polarised growth at the tips of the elongate yeast cells and a switch  
75 to cell division by septation without subsequent cell separation.

76

77 The conidia are the infectious propagules and infection is believed to be initiated  
78 through their inhalation (Vanittanakom et al. 2006). Once within the human host,  
79 *T. marneffe*i conidia are engulfed by host primary alveolar macrophages where  
80 they bypass the process of arthroconidiation and germinate directly into yeast  
81 cells, which are the pathogenic form. While hyphae and yeast are the  
82 predominant morphologies for *T. marneffe*i, particular growth conditions  
83 manifest distinct differences in cell shape and length for some cell types. For  
84 instance, *in vitro* grown *T. marneffe*i yeast cells have an elongated, filament-like  
85 morphology, whilst *in vivo* produced yeast cells are short, ellipsoid and compact,  
86 a form more suited for growing within the confines of the macrophage. As an  
87 intracellular pathogen the ability of *T. marneffe*i to tightly regulate the dimorphic  
88 switch and maintain yeast morphology in the host is crucial for pathogenicity.  
89 Therefore, temperature drives the dimorphic switch and host signals modify  
90 yeast cell morphogenesis.

91

92 In a number of animal and plant pathogenic fungal species, cell type specific  
93 morphogenesis is controlled by signalling pathways involving the small GTPase  
94 molecular switches and their accessory factors; guanine-nucleotide exchange  
95 factors (GEFs) and GTPase-activating proteins (GAPs) (reviewed in (Chant &  
96 Stowers 1995)). These play crucial roles in processes associated with cell shape  
97 such as control of polarized growth and cytoskeletal organisation. Rho-type GEFs  
98 are responsible for activating their small GTPase targets and their activity has  
99 been shown to regulate cytokinesis, cell wall integrity, antifungal resistance,  
100 viability, tissue invasive growth, mycotoxin production and virulence (Fuchs et  
101 al. 2007; Tang et al. 2005; Herrmann et al. 2014; Zhang et al. 2018). The majority  
102 of these studies have focused on GEFs containing canonical structural domains -  
103 a catalytic *Dbl* homology domain (DH) domain and an auxiliary plekstrin  
104 homology (PH) domain, excluding the contribution of GEFs with alternate  
105 domain structures (reviewed in Rossman et al. 2005).

106

107 In *T. marneffe*i, a number of small GTPases of the Ras superfamily and associated  
108 downstream effectors have been shown to influence morphogenesis of all cell  
109 types in specific and distinct patterns, during growth under both *in vitro* and *ex*

110 *vivo* (intracellular macrophage) growth conditions, by affecting polarity  
111 establishment and the differentiation of distinct cell types (Boyce &  
112 Andrianopoulos 2011). For example, the Cdc42 orthologue in *T. marneffeii*,  
113 encoded by *cflA*, is required for correct yeast and hyphal cell morphogenesis *in*  
114 *vitro*, as well as germination of conidia but does not affect the various cell types  
115 or differentiation of asexual development structures (conidiophores). Whereas  
116 the Rac orthologue, encoded by *cflB*, is important for hyphal cell morphogenesis  
117 and asexual development but not yeast cell morphogenesis (Boyce et al. 2001;  
118 Boyce et al. 2003). In addition, orthologues of the p21 activated kinases (PAK)  
119 Ste20 and Cla4, encoded by *pakA* and *pakB* respectively, are important for  
120 conidial germination and yeast cell morphogenesis at 37°C (Boyce &  
121 Andrianopoulos 2007; Boyce et al. 2009). In particular *pakB* exclusively affects  
122 the formation of yeast cells during intracellular growth, suggesting that the  
123 pathways controlling morphogenesis of *T. marneffeii in vitro* and during  
124 intracellular growth in host cells have some unique components that respond to  
125 distinct cues.

126

127 In a *T. marneffeii* expression profiling study examining genes expressed during  
128 growth inside macrophages, a gene was identified that was specifically  
129 upregulated inside murine macrophages and was predicted to encode a RhoGEF-  
130 like protein (Weerasinghe et al 2018 *in prep*). This previously uncharacterised  
131 gene that was named *msgA* (macrophage specific GEF-like A) is the only RhoGEF-  
132 like encoding gene in *T. marneffeii* to show this specific pattern of expression.  
133 While *MsgA* contains a DH domain, unlike canonical GEFs, a Bin-Amphiphysin-  
134 Rvs (BAR) domain replaces the PH domain. Proteins containing BAR domain  
135 have been shown to play various roles in membrane dynamics as well as  
136 interacting with small GTPases and many other proteins (Habermann 2004;  
137 Zimmerberg & McLaughlin 2004; Dawson et al. 2006; Peter et al. 2004). Deletion  
138 of *msgA* results in aberrant yeast morphology during macrophage infection but  
139 not during *in vitro* growth at 37°C. Induced overexpression of *msgA* during *in*  
140 *vitro* growth resulted in yeast cell formation mimicking that of growth inside  
141 macrophages. Mutational analysis showed that the BAR domain of *MsgA* is  
142 crucial in establishing correct yeast morphogenesis and localisation during

143 intracellular growth. Together these results define a novel host infection specific  
144 pathway that regulates intracellular morphogenesis in *T. marneffe*.

145

## 146 **Materials and methods**

### 147 *Molecular methods and plasmid construction*

148 *T. marneffe* genomic DNA was isolated as previously described (Borneman et al.  
149 2000). Southern and northern blotting was performed using Amersham Hybond  
150 N+ membrane and [ $\alpha$ - $^{32}$ P]dATP labelled probes by standard methods (Sambrook  
151 et al. 1989). Sequences of primers are provided in Supplementary Table 1.

152

153 Deletion constructs were created using a modified Gateway™ method (Boyce et  
154 al. 2012). The deletion construct of *msgA* was created using pHW7711  
155 containing the pDONR-*pyrG* cassette. Wildtype PCR product of *msgA*  
156 (PMAA\_089500) was generated with primers VV55 and VV56 and cloned into  
157 pBluescript II SK+ to generate pHW7897. To make the deletion construct,  
158 pHW7905, PCR primers VV57 and VV58 were used to generate an inverse PCR  
159 product for the Gateway™ reaction. To create a complementation construct,  
160 wildtype PCR product of *msgA* was cloned into the *niaD* targetting plasmid  
161 pHB7615 to generate pHW8053.

162

163 The overexpression allele *xyLP(p)::msgA* (pHW8056) was generated by PCR  
164 amplification of 2 kb of the 5' promoter and ORF regions of the *msgA* gene using  
165 WW78 and WW77 to create subclone pHW8069. An inverse PCR product of  
166 pHW8069 was generated by amplification with primers WW79 and WW42 that  
167 excluded the promoter region. Subsequently the *xyLP(p)* fragment PCR amplified  
168 from pHW8056 using H57 and H56 was phosphorylated and ligated to the  
169 inverse PCR fragment from pHW8069.

170

171 To generate the *msgA::mCherry* construct, pHW8053 was inverse PCR amplified  
172 using WW46 and WW57 and the resultant product was cut with *XbaI*. The  
173 *mCherry* fragment from pHW7911 was isolated by digestion with *SpeI/EcoRV*  
174 and this was ligated into the pHW8053 inverse PCR product to generate  
175 pHW7965.

176

177 To generate the *msgA<sup>ADH</sup>* and *msgA<sup>ABAR</sup>* domain deletion alleles, pHW8053 was  
178 inverse PCR amplified using WW59 and WW60 ( $\Delta$ DH), and WW44 and WW45  
179 ( $\Delta$ BAR), and the resulting products were phosphorylated and self-ligated to  
180 produce pHW7966 and pHW7964 respectively. To generate the  
181 *msgA<sup>ADH</sup>::mCherry* and *msgA<sup>ABAR</sup>::mCherry* the same primers were used to inverse  
182 PCR from pHW7965 to generate pHW7962 and pHW7963.

183

#### 184 *Fungal strains and media*

185 DNA-mediated transformation of *T. marneffei* was performed as previously  
186 described (Borneman et al. 2000). Strains used in this study are listed in  
187 Supplementary Table 2. Strains G816 ( $\Delta$ *ligD*::*pyrG*, *niaD1*) and G809  
188 ( $\Delta$ *ligD*::*pyrG*<sup>+</sup>, *niaD1*) were used as recipient strains to generate  $\Delta$ *msgA* and  
189 *xylP(p)::msgA* strains respectively (Bugeja et al. 2012). The  $\Delta$ *msgA* strain was  
190 generated by transforming G816 with the *XhoI/NotI* fragment of pHW7905 to  
191 delete *msgA* from -200 to +6040 (relative to the translational start).  
192 Transformants were selected for uracil prototrophy. The *xylP(p)::msgA* strain  
193 was generated by transforming G809 with the *NruI/EcoRV* fragment of  
194 pHW8056. Transformants were selected for glufosinate resistance. Strains  
195 bearing the *msgA*<sup>+</sup>, *msgA::mCherry*, *msgA<sup>ABAR</sup>*, *msgA<sup>ADH</sup>*, *msgA<sup>ABAR</sup>::mCherry* and  
196 *msgA<sup>ADH</sup>::mCherry* alleles in a  $\Delta$ *msgA* background were generated by  
197 transforming G1003 with pHW8055, pHW7965, pHW7966, pHW7964,  
198 pHW7962 and pHW7963 respectively. These constructs were targeted to the  
199 *niaD* locus to generate strains G1045, G1046, G1047, G1048, G1049 and G1050  
200 respectively. Homologous integration at *niaD* repairs the mutation in this strain,  
201 and transformants were selecting for their ability to utilise nitrate as a sole  
202 nitrogen source.

203

204 For induction of the *xylP* promoter during hyphal growth at 25°C *in vitro*, strains  
205 were grown in BHI medium with (inducing) or without (non inducing) 1% xylose  
206 for 4 days before microscopic observation. For growth in continuous inductive or  
207 non-inductive conditions, growth in each medium was extended for a further  
208 two days (total 6 days). For yeast growth at 37°C *in vitro*, strains were grown in

209 BHI medium for 4 days then transferred to BHI medium with (inducing) or  
210 without (non inducing) 1% xylose for a further 2 days. For growth in continuous  
211 inductive or non-inductive conditions, strains were grown for 6 days in BHI with  
212 or without 1% xylose respectively.

213  
214 In order to determine the septal span in hyphal cells for the wildtype and  
215 *xyLP(p)::msgA* during induced *msgA* expression, the distance between septa was  
216 measured for a 100 subapical cellular compartments for both strains.  
217 Additionally to determine the branching frequency for the wildtype and  
218 *xyLP(p)::msgA* during induced *msgA* expression, the number of branch points  
219 along a 100µm section of subapical hyphal cells for ten hyphae was counted for  
220 both strains.

221

#### 222 *Preparation of RNA*

223 RNA was isolated from two separate conditions for RT-PCR analysis. For the *in*  
224 *vitro* expression experiments RNA was isolated from FRR2161 (wildtype) yeast  
225 cells grown at 37°C for 6 days in liquid Brain Heart Infusion medium (BHI). For  
226 the macrophage infection expression experiments RNA was isolated from  
227 FRR2161 (wildtype) and  $\Delta$ *msgA* (G1003) cells isolated from infected  
228 lipopolysaccharide (LPS)(Sigma) activated J774 murine macrophages. J774  
229 murine macrophages were seeded at a concentration of  $1 \times 10^6$ /ml into 175cm<sup>3</sup>  
230 sterile cell culture flasks in 20 mL of complete Dulbecco's Modified Eagle  
231 Medium (DMEM, 10% foetal bovine serum, 8 mM L-glutamine and 1% penicillin-  
232 streptomycin), incubated at 37°C for 24 h and then activated with 0.1 µg/mL LPS  
233 for 24 h. Macrophages were washed in phosphate buffered saline (PBS) and 20  
234 mL of complete DMEM containing  $1 \times 10^7$  conidia was added. Macrophages were  
235 incubated for 2 h at 37°C (to allow conidia to be phagocytosed), washed once in  
236 PBS (to remove free conidia) and incubated a further 24 h at 37°C. Macrophages  
237 were then treated with 4 ml of 0.25% v/v Triton X solution for 2 minutes at room  
238 temperature to lyse the macrophages and extract *T. marneffe*. Both the lysate  
239 and *T. marneffe* grown in DMEM medium without macrophages were  
240 centrifuged at 2000 rpm for 5 minutes at 4°C. The resultant pellets were washed  
241 in PBS and the RNA was extracted using TRIzol Reagent (Invitrogen) and a MP



242 FastPrep-24 bead beater according to the manufacturer's instructions. RNA was  
243 DNase treated (Promega) prior to expression analysis.

244

#### 245 *Macrophage infection assay*

246 J774 murine or THP-1 human macrophages were seeded at a concentration of 1  
247  $\times 10^5$ /ml into a 6 well microtitre tray containing one sterile coverslip and 2 mL of  
248 complete DMEM (J774) or RPMI (THP-1) per well. J774 macrophages were  
249 incubated at 37°C for 24 h before activation with 0.1  $\mu$ g/mL LPS. THP-1  
250 macrophages were differentiated with 32 $\mu$ M phorbol 12-myristate 13-acetate  
251 (PMA) at 37°C for 24 h. Macrophages were incubated a further 24 h at 37°C,  
252 washed in PBS and 2 mL of DMEM or RPMI medium containing 1  $\times 10^6$  conidia  
253 was added. A control lacking conidia was also performed. Macrophages were  
254 incubated for 2 h at 37°C (to allow conidia to be engulfed), washed once in PBS  
255 (to remove free conidia) and incubated a further 24 or 48 h at 37°C after the  
256 addition of 2 mL of fresh DMEM or RPMI medium. Macrophages were fixed in 4%  
257 paraformaldehyde and stained with 1 mg/mL fluorescent brightener 28  
258 (calcofluor, CAL) to observe fungal cell walls. Mounted coverslips were examined  
259 using differential interference contrast (DIC) and epifluorescence optics for cell  
260 wall staining and viewed on a Reichart Jung Polyvar II microscope. Images were  
261 captured using a SPOT CCD camera (Diagnostic Instruments Inc) and processed  
262 in Adobe Photoshop™. The number of ungerminated conidia, germlings,  
263 filaments or yeast cells was recorded in a population of approximately 100  
264 macrophages in three independent experiments. Filaments were defined as any  
265 fungal cell with at least one septum. Ellipsoid and elongated fungal cells with no  
266 septa were counted as yeast cells. Mean and standard error of the mean values  
267 were calculated.

268

#### 269 *Microscopic techniques for morphological analysis of T. marneffeii*

270 For morphological and general growth examination, *T. marneffeii* was grown in  
271 liquid BHI (Oxoid) medium at 25°C for 2 days (hyphal growth) or 37°C for 4 days  
272 followed by transfer of approximately 10% of the culture to fresh medium for a  
273 further 2 days at 37°C (yeast growth). Aliquots of 500 $\mu$ L were transferred to 1.5  
274 mL microfuge tubes containing 20  $\mu$ L of 4% paraformaldehyde in PME (50 mM

275 piperazine-N, N'-bis(2-ethanesulfonic acid (PIPES), 1 mM MgSO<sub>4</sub>, 20 mM EGTA  
276 pH 6.7) fixing solution. Samples were incubated for 20 min at room temperature  
277 and then pelleted by centrifugation for 5 min. The supernatant was removed and  
278 pellets were resuspended in 0.001% v/v Tween 80 supplemented with  
279 fluorescent brightener 28 (final concentration 0.014 mg/mL) and observed  
280 microscopically.

281

### 282 *Immunofluorescence microscopy*

283 Immunofluorescence localization of the *msgA::mCherry*, *msgA<sup>ADH</sup>::mCherry* and  
284 *msgA<sup>ABAR</sup>::mCherry* strains was performed with anti-mCherry rat monoclonal  
285 primary antibody (Life Technologies) and an anti-rat ALEXA 488 conjugated goat  
286 secondary antibody (Molecular Probes) using standard protocols (Fischer &  
287 Timberlake 1995). Immunofluorescence microscopy controls using only primary  
288 or secondary antibodies as well as an untagged strain were performed to  
289 confirm specificity of the antibodies.

290

### 291 *Germination tests*

292 For *in vitro* germination experiments, approximately 10<sup>5</sup> spores were inoculated  
293 into 200 µl of Synthetic Dextrose (SD) medium containing 10 mM (NH<sub>4</sub>)<sub>2</sub>SO<sub>4</sub> and  
294 incubated for 8, 16, or 24 h at 37°C. The rates of germination were measured  
295 microscopically by counting the numbers of germinating conidia (conidia with a  
296 visible germ tube) in a population of approximately 100 fungal cells. Three  
297 independent experiments were performed. Mean and standard error of the mean  
298 values were calculated.

299

## 300 **Results**

301

### 302 *The msgA gene encodes a unique RhoGEF-like protein with a distinctive domain* 303 *structure and expression*

304 A previous RNAseq study identified the *msgA* gene as showing specific  
305 transcriptional upregulation during intracellular growth of *T. marneffei* in J774  
306 murine macrophages, relative to *in vitro* yeast or hyphal growth (Weerasinghe *et*  
307 *al.*, in prep). Based on this expression profile and its domain structure the gene

308 was denoted *msgA* (macrophage specific GEF-like). The *msgA* gene is one of six  
309 genes in the *T. marneffei* genome predicted to encode RhoGEF-like proteins.  
310 These are CtlA (Cdc24 orthologue), TusA (Tus1 orthologue), RomB (Rom1/Rom2  
311 orthologue), BudC (Bud3 orthologue) and RgfF (RhoGEF 6), based on the  
312 annotations in *Saccharomyces cerevisiae* (Cdc24, Tus1 and Rom1/Rom2),  
313 *Aspergillus nidulans* (Bud3) or having been previously undesignated (*msgA* and  
314 *rgfF*) (Figure 1A). RhoGEF proteins from a number of dimorphic and/or  
315 pathogenic fungi were examined and while orthologues of *MsgA* exist in many  
316 phyla they are absent from the Saccharomycotina sub-phylum and  
317 Basidiomycete phylum. It is also clear that *MsgA* is part of a distinct clade of  
318 RhoGEF-like proteins.

319

320 Canonical RhoGEFs are composed of two distinct domains, a Dbl homology  
321 domain (DH) which catalyses the exchange of GDP for GTP within Rho GTPases  
322 and a Plekstrin homology domain (PH) which assists in localisation of GEFs and  
323 regulation of their activity (reviewed in (Rossman et al. 2005)). Protein domain  
324 prediction analysis showed that *T. marneffei* RhoGEFs all contained a DH domain  
325 (Interpro ID: IPR000219) but showed differences in the composition of the  
326 second domain. CtlA, TusA and RgfF have PH domains (Interpro ID: IPR001849),  
327 while RomA and BudC lack a second domain. However *MsgA* has a Bin-  
328 Amphiphysin-Rvs (BAR) homology domain (Interpro ID: IPR004148)  
329 downstream of the DH domain (Figure 1A), and no PH domain. BAR domains are  
330 known to interact with membranes and sense and promote membrane curvature  
331 as well as act as a binding platform for GTPases (Takei et al. 1999),(Habermann  
332 2004). Additionally the predicted *MsgA* protein (1999 aa) is longer than other  
333 RhoGEFs, CtlA (932 aa), TusA (1781 aa), RomA (1217 aa), BudC (11546 aa) and  
334 RgfF (809 aa), and includes a large N-terminal region with no predicted domain  
335 motifs or localisation signals (Supplementary Figure 1A). This N-terminal  
336 sequence contains a 26 glutamic acid repeat (Supplementary Figure 1A). There is  
337 variation in the length of the acidic amino acid residue repeats in the *MsgA*  
338 orthologues from several clinical isolates of *T. marneffei*, ranging from 15 aa in  
339 isolates 3482 and 3841 to 26 aa in FRR 2161) (Supplementary Figure 1B). This is  
340 despite the high degree of sequence conservation outside this region.

341 Additionally this repeat is either greatly reduced or absent in closely related non-  
342 pathogenic, pathogenic and dimorphic species (Supplementary Figure 1B and C).  
343 The significance of these dynamic acidic amino acids strings is unclear at this  
344 stage. Tandem repeated sequences (TRSs) have previously been shown to affect  
345 adhesion and host immune system evasion in other fungi (Verstrepen et al. 2005;  
346 Verstrepen et al. 2004). A recent study of the genome structure of *T. marneffei*  
347 identified an increase in number of genes with TRSs compared to three other  
348 pathogenic and non-pathogenic filamentous fungi (Yang et al. 2013).

349

350 To examine the expression of the six genes encoding RhoGEF-like proteins in *T.*  
351 *marneffei*, including *msgA*, we queried the RNAseq analysis data (Weerasinghe *et*  
352 *al* in prep), which included gene expression profiles during *in vitro* hyphal  
353 growth at 25°C, *in vitro* yeast growth at 37°C, intracellular macrophage growth in  
354 J774 murine macrophages and THP-1 human macrophages, as well as growth in  
355 macrophage-free cell culture media. Most GEFs showed minimal (*ctlA*, *tusA* *budC*  
356 and *romA*) to no (*rgfF*) expression during yeast growth, either *in vitro* or during  
357 macrophage infection (Figure 1B). In contrast *msgA* showed upregulated  
358 expression specifically in the J774 macrophage infection condition, with a 13.4  
359 fold increase compared to the J774 *in media* condition. This data suggested that  
360 *msgA* might have a unique role during intracellular growth.

361

362 *MsgA is required for the formation of yeast inside host cells*

363 To characterise the role played by *msgA* during morphogenesis of *T. marneffei*,  
364 the gene was cloned, a deletion construct generated and this was used to create a  
365 deletion strain ( $\Delta msgA$ ) by DNA-mediated transformation. To confirm that any  
366 resulting phenotypes were caused by this gene deletion, the  $\Delta msgA$  strain was  
367 complemented with the wildtype (*msgA*<sup>+</sup>) allele targeted to the *niaD* locus. The  
368 wildtype (*msgA*<sup>+</sup>),  $\Delta msgA$  and  $\Delta msgA msgA^+$  strains were grown in liquid BHI  
369 medium at 25°C (hyphal) and 37°C (yeast) *in vitro* for 4 and 6 days respectively.  
370 At 25°C conidia from all three strains germinated normally and exhibited  
371 wildtype morphology, growing as polarized, branched septate hyphae. Similarly,  
372 at 37°C conidia from all three strains germinated and subsequently produced  
373 yeast cells (Figure 2A). Thus the  $\Delta msgA$  and  $\Delta msgA msgA^+$  strains were

374 indistinguishable from wildtype under *in vitro* growth conditions. This is  
375 consistent with the expression data in which the *msgA* transcript is present at  
376 very low levels during *in vitro* growth (Figure 1B).

377

378 When these stains were used to infect LPS activated J774 macrophages the  
379 wildtype and  $\Delta msgA$  *msgA*<sup>+</sup> strains were phagocytosed and germinated to  
380 produce small ellipsoid yeast cells that divided by fission after 24 h. In contrast  
381 macrophages infected with  $\Delta msgA$  conidia were equally phagocytosed but  
382 contained more branched, septate filamentous-like cells after 24 h (Figure 2B).  
383 Counts of the number of *T. marneffei* cells with at least one septum across  
384 approximately 100 infected macrophages showed that the wildtype and  $\Delta msgA$   
385 *msgA*<sup>+</sup> strains had 0.6±0.02% and 2.5±0.6% septate cells, respectively, while the  
386  $\Delta msgA$  strain had 37.4±0.49% septate cells. Concomitantly, the  $\Delta msgA$  strain  
387 showed a reduction in the number of yeast cells during macrophage infection  
388 with 55.8±1.85% compared to 81.8±1.89% and 86±0.56% in the wildtype and  
389  $\Delta msgA$  *msgA*<sup>+</sup> strains respectively. Longitudinal cell length measurements  
390 showed that yeast cells produced by the  $\Delta msgA$  strain were on average 1.4 times  
391 longer than both the wildtype and the  $\Delta msgA$  *msgA*<sup>+</sup> strains. This shows that  
392 *msgA* is important for correct yeast cell morphogenesis exclusively during  
393 macrophage infection.

394

395 Yeast cell morphogenesis *in vitro* occurs over days, rather than hours as seen  
396 inside host cells. So an explanation for the aberrant yeast cell morphology inside  
397 macrophages is that the cells are growing more slowly in the mutant. To test this  
398 hypothesis conidia of the wildtype,  $\Delta msgA$  and  $\Delta msgA$  *msgA*<sup>+</sup> strains were used  
399 to infect J774 macrophages and examined after extended incubation for 48 h  
400 post infection. At this time point macrophages infected with all three strains  
401 contain a large number of yeast cells dividing by fission. Macrophages infected  
402 with the wildtype or  $\Delta msgA$  *msgA*<sup>+</sup> strains showed similar yeast cell morphology  
403 that was short and oval shaped. In contrast, macrophages infected with the  
404  $\Delta msgA$  strain contained long and cylindrical yeast cells with at least one septum  
405 compared to the long multi septate, filaments observed at 24 h post infection  
406 (Figure 3A). The  $\Delta msgA$  strain yeast cells were 2.3 times longer than wildtype,

407 being  $8.9 \pm 0.57 \mu\text{m}$ , compared to wildtype and  $\Delta\text{msgA msgA}^+$  that were  
408  $3.9 \pm 0.12 \mu\text{m}$  and  $4.1 \pm 0.50 \mu\text{m}$  respectively (Figure 3B). As the  $\Delta\text{msgA}$  strain does  
409 not show germination defects either *in vitro* or during macrophage infection  
410 when compared to wildtype (Supplementary Table 3) and there are no  
411 morphological differences between the wildtype and  $\Delta\text{msgA}$  strains at 4, 6 or 8 h  
412 post-infection *ex vivo* (data not shown), the elongated yeast cell morphology  
413 observed in the  $\Delta\text{msgA}$  strain during macrophage infection is unlikely to reflect a  
414 delay in germination. Rather it points to a requirement of *msgA* in maintaining  
415 the compact, ellipsoid yeast cell morphology specific to macrophage infection.

416

417 *Aberrant morphogenesis of the msgA mutant is not due to defective host cell*  
418 *sensing*

419 The germination and morphogenesis of dormant conidia, which are produced  
420 during the hyphal growth phase at  $25^\circ\text{C}$ , into yeast cells differs *in vitro* compared  
421 to inside host cells. *In vitro* the conidia produce a polarised growth tip and  
422 generate multinucleate, multicellular hyphae before undergoing coupled nuclear  
423 and cell division to produce arthroconidiating hyphae. Fragmentation of these  
424 hyphae at septal junctions liberates uninucleate yeast cells. Inside host cells  
425 conidia undergo isotropic growth upon germination and form yeast cells directly.  
426 The morphology of  $\Delta\text{msgA}$  mutant cells in J774 macrophages resembled  
427 arthroconidiating hyphae, so one explanation for the mutant phenotype is that  
428 they can no longer accurately sense the host environment. To test this the  
429 expression of four genes known to be expressed at  $37^\circ\text{C}$  *in vitro*, but with little to  
430 no expression during J774 macrophage infection was examined (Weerasinghe *et*  
431 *al.*, in prep). RNA was extracted from the wildtype and  $\Delta\text{msgA}$  strains grown at  
432  $37^\circ\text{C}$  *in vitro* or during J774 macrophage infection and used for RT-PCR analysis.  
433 While the four genes showed a clear transcript in the wildtype grown at  $37^\circ\text{C}$  *in*  
434 *vitro*, no expression was observed during the J774 macrophage infection  
435 condition for either wildtype or  $\Delta\text{msgA}$  (Supplementary Figure 2). This suggests  
436 that the filaments and elongated yeast cells seen in the  $\Delta\text{msgA}$  strain are not  
437 similar to arthroconidial hyphae and yeast cells produced during wildtype  
438 growth *in vitro* at  $37^\circ\text{C}$ , and *msgA* has a specific role in maintaining cell shape  
439 during macrophage infection.

440

441 *MsgA also plays a role in the formation of yeast cells inside human cells*

442 The expression level of *msgA* in human THP-1 macrophages is very low  
443 compared to murine J774 cells at the 24h time point. To determine if the  
444 aberrant yeast cell morphogenesis phenotype of the  $\Delta msgA$  strain was limited to  
445 growth in J774 macrophages, THP-1 cells were infected with conidia from  
446 wildtype,  $\Delta msgA$  and  $\Delta msgA msgA^+$  strains and observed at 24 h post infection  
447 (Supplementary Figure 3A). The yeast cells displayed an increase in length  
448 ( $8.6 \pm 0.25 \mu\text{m}$ ) compared to wildtype ( $4.9 \pm 0.09 \mu\text{m}$ ) but were not as long, relative  
449 to wildtype, when growing inside J774 mouse cells (Supplementary Figure 3B).  
450 This suggests that *msgA* also plays a role in yeast cell morphogenesis inside THP-  
451 1 macrophages, albeit less pronounced.

452

453 *Overexpression of msgA produces aberrant hyphal morphology during growth at*  
454 *25°C*

455 The *msgA* gene is important for yeast cell morphogenesis in macrophages and  
456 shows very little expression at 25°C and 37°C *in vitro* (Figure 1A). In an attempt  
457 to gain more insight into the cellular activity of MsgA a construct that contained  
458 *msgA* under the control of a xylose inducible promoter, *xylP*, was generated and  
459 used to transform *T. marneffeii* strain G809 (Materials and methods). The  
460 wildtype and *xylP(p)::msgA*, strains were grown in BHI medium with (inducing)  
461 or without (non-inducing) 1% xylose (Materials and Methods). On non-inducing  
462 medium the *xylP(p)::msgA* strain was indistinguishable from wildtype at both the  
463 macroscopic and microscopic levels. On inducing medium the *xylP(p)::msgA*  
464 strain produced slightly swollen hyphae that displayed increased septation and  
465 hyper-branching along the hyphal length (Figure 4A). The distance between  
466 adjacent septa was  $38.6 \pm 0.9 \mu\text{m}$  for the wildtype,  $36.3 \pm 1.1 \mu\text{m}$  for the  $\Delta msgA$   
467 strain and  $6.6 \pm 0.18 \mu\text{m}$  for the *xylP(p)::msgA* strain. The frequency of branching  
468 in sub-apical cells along hyphae was  $1.15 \pm 0.11$  branches per 100  $\mu\text{m}$  of hyphal  
469 length for the wildtype,  $1.06 \pm 0.51$  for the  $\Delta msgA$  strain and  $11.05 \pm 0.81$  for the  
470 *xylP(p)::msgA* strain. Branching in apical cells was not observed in any of the  
471 strains and there was no significant difference in the nuclear index between  
472 these strains (data not shown). Extended incubation up to 6 days under inducing

473 conditions did not lead to the septate hyphae breaking down to form yeast cells.  
474 Therefore, the data shows that MsgA activity is required for specifying cell shape  
475 in host cells and can drive cell shape changes *in vitro*, possibly by affecting cell  
476 division.

477

478 *Overexpression of msgA at 37°C in vitro mimics yeast cell morphogenesis during*  
479 *macrophage infection*

480 Loss of *msgA* leads to the production of long and cylindrical yeast cells with *in*  
481 *vitro* morphology during macrophage infection rather than the wildtype short,  
482 ellipsoid cells. To test if MsgA could drive the development of the intracellular  
483 macrophage growth yeast cell morphology at 37°C *in vitro*, yeast cells from the  
484 wildtype and *xyLP(p)::msgA*, strains were transferred to BHI medium at 37°C  
485 both with (inducing) and without (non-inducing) 1% xylose (Materials and  
486 Methods). Under non-inducing conditions, the *xyLP(p)::msgA* strain was  
487 indistinguishable from wildtype, whereas on inducing medium the *xyLP(p)::msgA*  
488 strain produced yeast cells that were rounder and greatly reduced in length  
489 compared to wildtype (Figure 4B), resembling those produced by *T. marneffeii*  
490 during J774 macrophage infection (Figure 4B). These yeast cells also displayed  
491 patchy, uneven chitin staining. Additionally the arthroconidial filaments that  
492 produce these yeast cells display aberrant chitin deposition and an increased  
493 septation frequency immediately adjacent to the fission division sites (similar to  
494 the induced *xyLP(p)::msgA* strain at 25°C).

495

496 *In vitro* generated yeast cells consist of a mixture of arthroconidia (single cells  
497 formed by the separation of hyphal cells) and *bona fide* yeast cells  
498 (arthroconidial cells that have divided at least once). To determine if MsgA could  
499 drive the development of yeast cells directly from conidia at 37°C *in vitro*, as  
500 happens inside host cells, conidia from the wildtype,  $\Delta msgA$  and *xyLP(p)::msgA*  
501 strains were grown under continuous induction in BHI medium with 1% xylose.  
502 After 6 days the wildtype and  $\Delta msgA$  strains produce elongated yeast cells under  
503 both inducing and non-inducing conditions. In contrast, the *xyLP(p)::msgA* strain  
504 produced small ellipsoid yeast cells similar to those observed when *T. marneffeii*  
505 is growing inside host cells (Supplementary Figure 4). These yeast cells appear



506 to be derived from swollen arthroconidial filaments rather than directly from  
507 conidia. Additionally, wildtype yeast cell formation occurs by fission driven  
508 separation from either pole of the primary yeast cell (Supplementary Figure 4).  
509 However, under continuous induction the *xylP(p)::msgA* strain produces a  
510 proportion of aberrantly shaped yeast cells, with uneven chitin deposition, that  
511 appear to produce yeast cells from multiple fission sites at the poles, often  
512 resulting in the production of two yeast cells from a single pole (Figure 4C).  
513 Sometimes these aberrant yeast cells, as well as long filamentous cells, produce  
514 cells that have lost their ellipsoid shape and seem to be dividing by budding  
515 rather than fission (Figure 4D). Thus while the overexpression of *msgA in vitro* is  
516 able to recapitulate the phenotype of *T. marneffei* yeast cells grown within  
517 macrophages, continuous overexpression impedes yeast cell growth polarisation  
518 and results in inappropriate division.

519

#### 520 *The MsgA protein is involved in conidial production during asexual development*

521 During asexual development at 25°C, wildtype *T. marneffei* colonies are  
522 composed of vegetative hyphae that produce asexual differentiated structures  
523 (conidiophores) from which green-pigmented asexual spores (conidia) are  
524 generated by basipetal budding (Borneman et al. 2000). The  $\Delta msgA$  mutant  
525 strain produced fewer conidia than wildtype, resulting in a paler colonial  
526 appearance (Supplementary Figure 5A). Conidial counts of wildtype,  $\Delta msgA$  and  
527  $\Delta msgA msgA^+$  strains revealed that the  $\Delta msgA$  strain produced  $5.3 \times 10^8 \pm 0.4$   
528 conidia/ml while the wildtype produced  $23.9 \times 10^8 \pm 0.9$  conidia/ml. The  
529 complemented  $\Delta msgA msgA^+$  strain did not completely rescue the phenotype of  
530 the  $\Delta msgA$  mutant strain with conidiation levels at  $15.9 \times 10^8 \pm 1.1$  conidia/ml  
531 (Supplementary Figure 5B). The complementation allele included 891 bp of  
532 promoter sequence, however examination of the 3624 bp region between the  
533 *msgA* start codon and the upstream gene (PMAA\_089490) identified four  
534 putative recognition sites for asexual development transcriptional regulators  
535 BrlA (5'-MRAGGGT-3', at -1162 and -3067) and AbaA (5'-CATTCY-3' at -339 and  
536 -1711). Of these only one (AbaA at -339) site was within the region included in  
537 the reintroduced allele. This may explain the partial complementation observed  
538 in the  $\Delta msgA msgA^+$  strain. A similar phenotype has been observed for the *drkA*

539 gene in *T. marneffei*, which was attributed to the absence of BrlA and AbaA  
540 recognition sites (Boyce et al. 2011).

541

542 To test this hypothesis conidial density of the *msgA* over expression strain  
543 (*xylP(p)::msgA*) was measured with and without induction. In the absence of  
544 induction the number of conidia produced the *xylP(p)::msgA* strain was  
545 comparable to the  $\Delta msgA$  mutant strain, being  $7.7 \times 10^8 \pm 0.8$  conidia/ml. However  
546 in the presence of 0.5% xylose induction the conidiation level in the  
547 *xylP(p)::msgA* strain was  $35.2 \times 10^8 \pm 1.5$  conidia/ml, which is comparable to  
548 wildtype which produced  $33 \times 10^8 \pm 1.5$  conidia/ml (Supplementary Figure 5B).  
549 This suggests that promoter elements excluded in the *msgA*<sup>+</sup> complementation  
550 allele are necessary for the proper expression of *msgA* during asexual  
551 development, and highlights a role for *msgA* during conidial production.

552

553 *MsgA shows cell membrane localisation during macrophage growth.*

554 To investigate the localization of MsgA, the mCherry coding sequence was  
555 inserted into the C-terminal end of MsgA, after the DH domain. The  
556 *msgA::mCherry* fusion construct was targeted to the *niaD* locus in the  $\Delta msgA$   
557 (G1003) strain. This strain was used to infect J774 murine macrophages and  
558 wildtype yeast cell morphology was evident after 24 h showing that the fusion  
559 allele complemented the  $\Delta msgA$  phenotype during macrophage infection (Figure  
560 5A). Immunostaining of these infected cells with an anti-mCherry antibody and  
561 calcofluor co-staining showed that MsgA-mCherry specifically localized to yeast  
562 cells but not to ungerminated conidia (Figure 5B). Localization was observed  
563 around the cell periphery and in distinct punctate vesicular structures within the  
564 cytoplasm. Colocalization with calcofluor stained cell walls and septa was not  
565 observed, either at nascent septation sites prior to, or immediately after, cell wall  
566 deposition (Figure 5B-C). However localization of MsgA was observed in the  
567 region immediately adjacent to the cell wall during cell separation (Figure 5D-E).  
568 Brighter punctate structures of MsgA localization can be seen at the sites of  
569 cytokinesis in cells that are actively undergoing fission division. Thus MsgA is  
570 localised to the cell membrane and vesicles during macrophage infection, with an  
571 increased presence at cell division sites late in the cell division process.

572

573 *The BAR domain of MsgA is essential for proper yeast morphogenesis during*  
574 *macrophage infection*

575 In order to examine the role of the conserved domains of MsgA in the  
576 phenotypes observed during macrophage infection, mutant alleles were  
577 generated which deleted the DH (*msgA<sup>ΔDH</sup>*) or BAR domains (*msgA<sup>ΔBAR</sup>*). Domain  
578 deletion constructs were targeted to the *niaD* locus of the *ΔmsgA* (G1003) strain.  
579 These mutant strains were compared to the wildtype, the original deletion strain  
580 (*ΔmsgA*) and the wildtype complementation strain (*ΔmsgA msgA<sup>+</sup>*). Both the  
581 *msgA<sup>ΔDH</sup>* and *msgA<sup>ΔBAR</sup>* strains were indistinguishable from the control strains  
582 during *in vitro* growth at 25°C and 37°C (data not shown). When conidia from  
583 these strains were used to infect LPS activated J774 murine macrophages  
584 numerous yeast cells that were dividing by fission were present for the wildtype,  
585 *ΔmsgA msgA<sup>+</sup>* and *msgA<sup>ΔDH</sup>* strains after 24 h. In contrast macrophages infected  
586 with *ΔmsgA* and *msgA<sup>ΔBAR</sup>* strains contained both septate yeast as well as long  
587 septate filament cells (Figure 6A). Macrophages infected with the *msgA<sup>ΔBAR</sup>* strain  
588 contained 39.1±0.6% filaments of the total fungal load when compared to the  
589 *msgA<sup>ΔDH</sup>* strain, which contained 0.8±0.4% filaments (Figure 6B). Similar to the  
590 *ΔmsgA* strain, the *msgA<sup>ΔBAR</sup>* strain contained fewer yeast cells compared to the  
591 *msgA<sup>ΔDH</sup>* and wildtype strains (Figure 6B). Here the *msgA<sup>ΔBAR</sup>* strain produced  
592 59.1±2.7% yeast cells compared to 84.4±0.5% formation rate in the *msgA<sup>ΔDH</sup>*  
593 strain. Thus the *msgA<sup>ΔBAR</sup>* allele did not complement the *ΔmsgA* mutation,  
594 indicating that the BAR domain is essential for normal yeast morphogenesis  
595 during macrophage infection. Both domain deletion alleles were also introduced  
596 into the wildtype strain but did not alter the wildtype phenotype under either  
597 the *in vitro* or intracellular macrophage growth conditions tested, suggesting that  
598 these alleles do not have a dominant interfering effect on the function of MsgA  
599 (data not shown).

600

601 To assess whether the DH or BAR deletion mutations affect the localization of  
602 MsgA during macrophage infection, mCherry tagged *msgA<sup>ΔDH</sup>* and *msgA<sup>ΔBAR</sup>*  
603 constructs were generated and targeted to the *niaD* locus in the *ΔmsgA* (G1003)  
604 strain. These strains were used to infect J774 murine macrophages and, as

605 observed for the non-mCherry fusion alleles, wildtype yeast cell morphology was  
606 evident after 24 h for the *msgA*<sup>ΔDH</sup>::mCherry allele but not for the  
607 *msgA*<sup>ΔBAR</sup>::mCherry allele (Figure 7). Immunostaining of these infected cells with  
608 an anti-mCherry antibody and calcofluor co-staining showed that the localisation  
609 pattern for the *MsgA*<sup>ΔDH</sup>-mCherry was the same as that of the *MsgA*-mCherry  
610 with punctate localisation in the cytoplasm and at the cell membrane and none at  
611 the cell wall either during cell wall deposition at the septa or during cytokinesis.  
612 In contrast, the *MsgA*<sup>ΔBAR</sup>-mCherry gene product showed mislocalisation to the  
613 cell wall where it co-staining with calcofluor. The *MsgA*<sup>ΔBAR</sup>-mCherry gene  
614 product did not show the punctate pattern of localisation within the cytoplasm  
615 like wildtype and was not localized to nascent septation sites prior to or  
616 immediately after cell wall deposition (Figure 7). However *MsgA*<sup>ΔBAR</sup>-mCherry  
617 showed weak localisation at the cell wall of septation sites during cell separation  
618 (Figure 7). This suggests the possible late recruitment of *MsgA* to the cell  
619 separation complex.

620

## 621 Discussion

622 Survival and proliferation of microbial pathogens in a host relies on their ability  
623 to cope with host defence mechanisms and acquire nutrients for growth. For a  
624 number of prokaryotic and eukaryotic microbial pathogens this is coupled with  
625 the ability to grow inside cells of the host. In intracellular dimorphic pathogenic  
626 fungi, the ability to switch from a multicellular hyphal growth form into a  
627 unicellular yeast form that is more spatially suited to residing within host cells, is  
628 crucial for pathogenicity (Nemecek et al. 2006; Webster & Sil 2008; Beyhan et al.  
629 2013). An important inducer of this switch is a shift to 37°C (mammalian body  
630 temperature), and this coincides with the conversion of infectious propagules to  
631 a pathogenic form. This study examined a previously uncharacterised *Dbl*  
632 homology/BAR domain protein encoded by *msgA*, which is strongly upregulated  
633 in the dimorphic, human-pathogenic fungus *T. marneffeii* during J774 murine  
634 macrophage infection and is critical for yeast morphogenesis in macrophages. It  
635 was demonstrated that *msgA* does not play a role *in vitro*, during yeast or hyphal  
636 cell morphogenesis at either 37°C or 25°C, but does affect asexual development.  
637 Factors that are important for both yeast cell morphogenesis and asexual

638 development have been identified previously. In particular studies of the cell  
639 signalling pathways in *T. marneffeii* have uncovered similar effects for PakB, the  
640 *CLA4* homologue encoding a p21-activated kinase, in yeast cell formation  
641 particularly during macrophage growth (Boyce & Andrianopoulos 2007).  
642 Together the data indicate that morphogenesis in *T. marneffeii* during infection  
643 may respond to a host internalisation triggered mechanism that induces the  
644 expression of *msgA* and other associated genes, and that the activation of this  
645 pathway drives cellular processes that responds to the host environment.

646

#### 647 *MsgA is involved in intracellular morphogenesis*

648 The *msgA* gene has a unique expression profile that foreshadows its contribution  
649 to yeast cell morphogenesis during macrophage infection. In comparison to the  
650 other six *Rho* GEF encoding genes, *msgA* shows high level and specific expression  
651 in *T. marneffeii* during J774 murine macrophage infection. Consistent with this  
652 expression pattern the *msgA* deletion strain displayed septate and branched  
653 filament production during intracellular growth but wildtype yeast cell  
654 morphogenesis *in vitro* at 37°C. These aberrant *ex vivo* generated filaments were  
655 morphologically more similar to arthroconidia/yeast cells produced at 37°C *in*  
656 *vitro* but they failed to show expression of a number of genes known to be  
657 expressed exclusively in *in vitro* generated yeast cells, suggesting that the defect  
658 is unlikely to be the result of a failure to detect the local environment. A similar,  
659 albeit less severe, phenotype was observed when THP-1 human macrophages  
660 were used. An alternative explanation for the morphogenesis defect is that the  
661 phagocytosed conidia germinate aberrantly, however kinetic studies of  
662 germination for the *msgA* deletion strain failed to identify any differences  
663 compared to the wildtype under any condition. Coupled with the observation  
664 that overexpression of *msgA* at 37°C *in vitro* drives the formation of shorter  
665 ellipsoid yeast cells that resemble yeast during intracellular macrophage growth  
666 suggests that *msgA* is a key determinant of cell shape and identity and is  
667 sufficient to redirect cellular morphogenetic programs towards infection-specific  
668 yeast cell formation.

669

670 Unlike other dimorphic pathogens where the yeast phase is marked by budding  
671 division, *T. marneffeii* yeast cells divide by fission, so yeast and hyphal cells share  
672 the polarised growth characteristics, up to the point of cell division. At cell  
673 division hyphal cells lay down a cell wall to generate a new cell compartment  
674 with no associated cell separation, whilst yeast cells undergo cell separation. The  
675 formation of elongated, filament-like yeast cells that are sometimes multiseptate  
676 by the  $\Delta msgA$  mutant strain during infection points to a disruption in the  
677 coordination of these processes and suggests that MsgA plays a vital role in  
678 processes that involve cell division (septation) and cell separation. While its  
679 precise role remains to be determined, the redistribution of MsgA from the  
680 entire cell membrane to that adjacent to the newly formed septum and before  
681 cell separation suggests that it is involved more at the cell separation stage than  
682 septation. The smaller, ellipsoid yeast cells produced by overexpressing *msgA* at  
683 37°C *in vitro* and the defect in conidiogenesis for the  $\Delta msgA$  mutant strain are  
684 both consistent with this hypothesis that *msgA* is important for cell division and  
685 separation. Additionally, overexpressing *msgA* at 25°C *in vitro* results in increased  
686 septation along the hyphae producing shorter cellular compartments. Unlike  
687 yeast cell growth these compartments do not separate into individual cells,  
688 which is probably due to the absence of expression and/or activity of the yeast-  
689 specific machinery necessary for separation.

690

691 It is clear that *msgA* plays a fundamental role in the morphogenesis of yeast cells  
692 growing inside host cells and for conidial production during asexual  
693 development. The *pakB* gene of *T. marneffeii*, encoding a p21-activated kinase,  
694 also plays an important role in cell division of yeast cells in macrophages and  
695 affect asexual development. *In vitro* overexpression of *pakB* alleles with either a  
696 mutated CRIB (Cdc42/Rac Interactive Binding) or GBB (Gβ binding) domains,  
697 results in the production of yeast cells that resembled those produced during  
698 growth inside macrophages (Boyce et al. 2009). Additionally MsgA and PakB  
699 have complementary localisation patterns at septation sites during intracellular  
700 yeast formation. Together these are suggestive of coordinated effects on  
701 morphogenetic mechanisms that involve the regulation of cell division. Similar  
702 localization and morphological function has been observed in *S. cerevisiae* for the

703 GEF-like protein Lte1, which plays a vital role in activating the Mitotic Exit  
704 Network (MEN) and the formation of daughter bud cells. Lte1 is localized to the  
705 incipient bud cortex and *lte1* mutants show delayed cytokinesis and aberrant  
706 daughter cell morphology (Bertazzi et al. 2011; Geymonat et al. 2009). Lte1 is  
707 activated by the PakB homologue Cla4, which enables its localisation to the bud  
708 where it inhibits machinery that prevents mitotic exit and thus proper bud  
709 formation (Höfken & Schiebel 2002; Jensen et al. 2002; Seshan et al. 2002;  
710 Yoshida et al. 2003). In this respect LTE1 does not function as a GEF but rather in  
711 a separate signalling pathway controlling morphogenesis. *T. marneffei* and other  
712 filamentous fungi lack a clear, conserved orthologues of Lte1 and components  
713 involved in MEN, suggesting that they use an alternate pathway to accomplish  
714 this role and this may include the MsgA and PakB.

715

#### 716 *Unique domain structure of MsgA influences its function and localisation*

717 The predicted gene product of *msgA* possesses a DH domain stereotypical of  
718 GEFs and involved in regulating GTP dependent interactions. However it lacks  
719 the auxiliary PH domain that is common to canonical GEFs and important for  
720 localisation. Instead MsgA has a BAR domain that is not present in any of the  
721 other Ras, Rho, Rsr, Arf, Rab and Ran GEFs in *T. marneffei*, but which is conserved  
722 in orthologues of MsgA in other ascomycete fungi. The function of the BAR  
723 domain has been characterised in a number of systems and it is clear that it is  
724 involved in membrane dynamics, particularly by its ability to oligomerise and  
725 induce membrane bending, but can also bind small GTPases and affect their  
726 function (Habermann 2004). The data shows that a *msgA* allele missing the BAR  
727 domain (*msgA*<sup>ΔBAR</sup>) failed to complement the aberrant yeast morphology  
728 phenotype observed in the  $\Delta$ *msgA* strain whereas a *msgA* allele missing the DH  
729 domain (*msgA*<sup>ΔDH</sup>) fully rescued this phenotype. At least part of basis for this lack  
730 of complementation is likely to be due to the resultant loss of localisation of  
731 MsgA when the BAR domain is removed. This hypothesis is consistent with the  
732 correct localisation, and complementation, of the MsgA mutant protein that  
733 contains the BAR domain but lacks the DH domain. Like a number of other BAR  
734 domain proteins this suggests that part of its role may reside in its interaction

735 with, and recruitment of, other factors to specific sites on the cell membrane  
736 (Miki et al. 2000; Schorey et al. 1997).

737

738 Proteins containing BAR domains are known to interact with many small  
739 GTPases including Rac (Tarricone et al. 2001; Van Aelst et al. 1996; Schorey et al.  
740 1997). In *T. marneffeii* the Rac- (*cflB*), Cdc42- (*cflA*) and Ras- encoding (*rasA*)  
741 genes have been shown to play important and distinct roles in hyphal and yeast  
742 morphogenesis *in vitro*, yeast morphogenesis *ex vivo*, conidial germination and  
743 asexual development (Boyce et al. 2001; Boyce et al. 2003; Boyce et al. 2005), yet  
744 none of the phenotypes associated with the various mutant alleles examined in  
745 these studies, which include deletion, dominant activating and negative alleles,  
746 mimic those for *msgA* alleles. The *rasA*, *cflA* and *msgA* genes play a role in yeast  
747 cell morphogenesis but the *msgA* effects are restricted to *ex vivo* yeast while the  
748 *rasA* and *cflA* effects occur in all yeast cells. Moreover, the phenotypes of the  
749 *msgA* and *rasA/cflA* mutants with respect to yeast morphology are strikingly  
750 different. Similarly, the *cflB* and *msgA* genes play a role in asexual development  
751 but the effects of perturbing their function are different. Coupled with the  
752 observation that deletion of the DH domain does not appear to affect *MsgA*  
753 function and that *msgA* mutant yeast cells do not express *in vitro* yeast cell-  
754 specific genes, it seems that *msgA* controls yeast cell morphogenesis  
755 independently of these small GTPases and does not function in host recognition  
756 and signalling.

757

758 Canonical Rho GEFs have been investigated in a number of pathogenic fungi, and  
759 shown to play roles in cellular morphogenesis and pathogenicity (Wendland &  
760 Philippsen 2001; Bassilana et al. 2003; Fuchs et al. 2007; Tang et al. 2005).  
761 Similarly, non-GEF-like BAR domain proteins have been associated with  
762 morphology and virulence in a number of plant and human pathogenic fungi. For  
763 example, *C. albicans* *rvs* mutants affect hyphal morphogenesis, invasive growth  
764 and antifungal resistance through their involvement in endocytic mechanisms  
765 (Douglas et al. 2009). Also the rice blast fungus *M. oryzae* BAR domain proteins  
766 *Rvs161* and *Rvs167* are important for plant invasion through appressorial  
767 formation (Dagdas et al. 2012). However non-canonical GEF-like proteins with a



768 BAR domain are poorly understood in most systems, including fungi. The best  
769 example of a DH domain protein with an associated BAR domain is the human  
770 dynamin-binding scaffold protein Tuba, which localizes to brain synapses as  
771 puncta at the base of membrane ruffles and is involved in synaptic vesicle  
772 endocytosis (Salazar et al. 2003; Kovacs et al. 2006). Membrane ruffling plays a  
773 crucial role in internalization during substrate acquisition and receptor  
774 availability control as well as cell motility (Hoon et al. 2012). Deletion of the BAR  
775 domain in this Tuba abolishes dorsal ruffling of synaptic membranes and causes  
776 the mislocalisation of this protein throughout the cytoplasm, suggesting that the  
777 BAR domain is necessary for facilitating correct localisation of Tuba during  
778 synaptic cell cytoskeletal dynamics (Kovacs et al. 2006). The phenotypic  
779 similarities between MsgA and this distantly related mammalian protein are  
780 striking and support the idea that BAR domains are important factors in  
781 determining cellular morphology across kingdoms.

782

783 Analysis of the *msgA* gene of *T. marneffeii* shows that it is important for yeast cell  
784 morphogenesis during macrophage infection and in conidial production during  
785 asexual development. Although yeast cells divide by fission and conidia are  
786 formed by budding, both of these cell types require cell separation, which is  
787 unlike hyphal cells. Yeast cells formed *in vitro* also require cell separation but  
788 *msgA* does not appear to be required for this process. The distinction here may  
789 lie in the fact that yeast cell morphogenesis *in vitro* is always preceded by hyphal  
790 growth and the process of arthroconidiation that produces yeast cells *in vitro*  
791 may be mechanistically distinct. The data presented here suggests that *msgA* and  
792 the p21-activated kinase encoding *pakB* may function in the same pathway to  
793 control morphogenesis during infection. Further studies to identify binding  
794 partners of MsgA will shed light on the mechanism that controls cellular  
795 morphogenesis of *T. marneffeii* during infectious growth.

796

797 **References**

- 798 Andrianopoulos, A. (2002). Control of morphogenesis in the human fungal  
799 pathogen *Penicillium marneffe*. *Intl J Med Microbiol.* 292, 331–347.
- 800 Bassilana, M., Blyth, J. and Arkowitz, R.A. (2003). Cdc24, the GDP-GTP exchange  
801 factor for Cdc42, is required for invasive hyphal growth of *Candida albicans*.  
802 *Eukaryot Cell.* 2, 9–18.
- 803 Bertazzi, D.T., Kurtulmus, B. and Pereira, G. The cortical protein Lte1 promotes  
804 mitotic exit by inhibiting the spindle position checkpoint kinase Kin4. *J Cell*  
805 *Biol.* 193, 1033-1048.
- 806 Beyhan, S., Gutierrez, M., Voorhies, M. and Sil, A. (2013). A temperature-  
807 responsive network links cell shape and virulence traits in a primary fungal  
808 pathogen J. *PLoS Biol.* 11(7), e1001614.  
809
- 810 Borneman, A. R., Hynes, M. J. and Andrianopoulos, A. (2000). The *abaA*  
811 homologue of *Penicillium marneffe* participates in two developmental  
812 programmes: conidiation and dimorphic growth. *Mol. Microbiol.* 38(5),  
813 1034–(1047).
- 814 Boyce, K. J. and Andrianopoulos, A. (2007). A p21-activated ainase is required for  
815 conidial germination in *Penicillium marneffe*. *PLOS Pathog.* 3(11), e162.
- 816 Boyce, K. J. and Andrianopoulos, A. (2011). Ste20-related kinases: effectors of  
817 signaling and morphogenesis in fungi. *Trends Microbiol.* 19(8), 400–410.
- 818 Boyce, K. J., Bugeja H. E., Weerasinghe, H., Payne, M. J., Schreider, L., Park, C.,  
819 Woodward, T. and Andrianopoulos, A. (2012). Strategies for the molecular  
820 genetic manipulation and visualization of the human fungal pathogen  
821 *Penicillium marneffe*. *Fungal Genet Rep.* 59(1), 1–12.
- 822 Boyce, K. J., Schreider, L., Kirszenblat, L. and Andrianopoulos, A. (2011). The two-  
823 component histidine kinases DrkA and SlnA are required for *in vivo* growth  
824 in the human pathogen *Penicillium marneffe*. *Mol. Microbiol.* 82(5), 1164–  
825 1184.
- 826 Boyce, K. J., Hynes, M. J. and Andrianopoulos, A. (2003). Control of  
827 morphogenesis and actin localization by the *Penicillium marneffe* RAC  
828 homolog. *J. Cell Sci.* 116(7), 1249–1260.
- 829 Boyce, K.J., Hynes, M. J. and Andrianopoulos, A. (2001). The CDC42 homolog of  
830 the dimorphic fungus *Penicillium marneffe* is required for correct cell  
831 polarization during growth but not development. *J. Bacteriol.* 183(11), 3447–  
832 3457.
- 833 Boyce, K. J., Hynes, M. J. and Andrianopoulos, A. (2005). The Ras and Rho  
834 GTPases genetically interact to co-ordinately regulate cell polarity during  
835 development in *Penicillium marneffe*. *Mol. Microbiol.* 55(5), 1487–1501.
- 836 Boyce, K. J., Schreider, L. and Andrianopoulos, A. (2009). *In vivo* yeast cell

- 837 morphogenesis is regulated by a p21-activated kinase in the human  
838 pathogen *Penicillium marneffe*. *PLoS Pathog.* 5(11), e1000678.
- 839 Brandhorst, T.T., Wüthrich, M., Warner, T. and Klein, B. (1999). Targeted gene  
840 disruption reveals an adhesin indispensable for pathogenicity of *Blastomyces*  
841 *dermatitidis*. *J. Expt Med.* 189(8), 1207–1216.
- 842 Bugeja, H. E., Boyce, K. J., Weerasinghe, H., Beard, S., Jeziorowski, A., Pasricha, S.,  
843 Payne, M.J., Schreider, L. and Andrianopoulos, A. (2012). Tools for high  
844 efficiency genetic manipulation of the human pathogen *Penicillium marneffe*.  
845 *Fungal Genet Biol.* 49(10), 772–778.
- 846 Chant, J. and Stowers, L. (1995). GTPase cascades choreographing cellular  
847 behavior: Movement, morphogenesis, and more. *Cell.* 81(1), 1–4.
- 848 Dagdas, Y. F., Yoshino, K., Dagdas, G., Ryder, L. S., Bielska, E., Steinberg, G. and  
849 Talbot, N. J. (2012). Septin-mediated plant cell invasion by the rice blast  
850 fungus, *Magnaporthe oryzae*. *Science.* 336(6088), 1590–1595.  
851
- 852 Dawson, J. C., Legg, J. A. and Machesky, L. M. (2006). Bar domain proteins: a role  
853 in tubulation, scission and actin assembly in clathrin-mediated endocytosis.  
854 *Trends Cell Biol.* 16(10), 493–498.
- 855 Douglas, L. M., Martin, S. W. and Konopka, J. B. (2009). BAR domain proteins  
856 Rvs161 and Rvs167 contribute to *Candida albicans* endocytosis,  
857 morphogenesis, and virulence. *Infect. Immun.* 77(9), 4150–4160.
- 858 Fischer, R. and Timberlake, W. E. (1995). *Aspergillus nidulans* *apsA* (anucleate  
859 primary sterigmata) encodes a coiled-coil protein required for nuclear  
860 positioning and completion of asexual development. *J. Cell Biol.* 128(4), 485–  
861 498.
- 862 Fuchs, B. B., Tang, R. J. and Mylonakis, E. (2007). The temperature-sensitive role  
863 of *Cryptococcus neoformans* ROM2 in cell morphogenesis. *PLoS One*, 2(4),  
864 e368.
- 865 Geymonat, M., Spanos, A., de Bettignies, G. and Sedgwick, S. G. (2009). Lte1  
866 contributes to Bfa1 localization rather than stimulating nucleotide exchange  
867 by Tem1. *J. Cell Biol.* 187(4), 497–511.  
868
- 869 Habermann, B. (2004). The BAR-domain family of proteins: a case of bending  
870 and binding? *EMBO Reps*, 5(3), 250–255.
- 871 Herrmann, A., Herrmann, A., Tillmann, B. A. M., Schürmann, J., Bölker, M. and  
872 Tudzynski, P. (2014). Small-GTPase-associated signaling by the guanine  
873 nucleotide exchange factors CpDock180 and CpCdc24, the GTPase effector  
874 CpSte20, and the scaffold protein CpBem1 in *Claviceps purpurea*. *Eukaryot*  
875 *Cell.* 13(4), 470–482.  
876
- 877 Hoon, J.-L., Wong, W.-K. and Koh, C.-G. (2012). Functions and regulation of  
878 circular dorsal ruffles. *Mol. Cell Biol.* 32(21), 4246–4257.

- 879 Höfken, T. and Schiebel, E. (2002). A role for cell polarity proteins in mitotic exit.  
880 *EMBO J.* 21(18), 4851–4862.
- 881 Jensen, S., Geymonat, M., Johnson, A. L., Segal, M. and Johnston, L. H. (2002).  
882 Spatial regulation of the guanine nucleotide exchange factor Lte1 in  
883 *Saccharomyces cerevisiae*. *J. Cell Sci.*, 115(24), 4977–4991.  
884
- 885 Kovacs, E. M., Makar, R. S. and Gertler, F. B. (2006). Tuba stimulates intracellular  
886 N-WASP-dependent actin assembly. *J. Cell Sci.* 119(13), 2715–2726.
- 887 Miki, H., Yamaguchi, H., Suersigi, S. and Takenawa, T. (2000). IRSp53 is an  
888 essential intermediate between Rac and WAVE in the regulation of  
889 membrane ruffling. *Nature*, 408(6813), 732–735.
- 890 Nemecek, J. C., Wüthrich, M. and Klein, B.S. (2006). Global control of dimorphism  
891 and virulence in fungi. *Science*, 312(5773), 583–588.
- 892 Nguyen, V. Q. and Sil, A. (2008). Temperature-induced switch to the pathogenic  
893 yeast form of *Histoplasma capsulatum* requires Ryp1, a conserved  
894 transcriptional regulator. *Proc. Natl. Acad. Sci. USA*, 105(12), 4880–4885.
- 895 Peter, B. J., Kent, H. M., Mills, I. G., Vallis, Y., Buttler, P. J., Evans, P. R. and  
896 McMahon, H. T. (2004). BAR domains as sensors of membrane curvature:  
897 The amphiphysin BAR structure. *Science*, 303(5657), 495–499.
- 898 Rooney, P. J., Sullivan, T. D. and Klein, B. S. (2001). Selective expression of the  
899 virulence factor BAD1 upon morphogenesis to the pathogenic yeast form of  
900 *Blastomyces dermatitidis*: evidence for transcriptional regulation by a  
901 conserved mechanism. *Mol. Microbiol.* 39(4), 875–889.
- 902 Rossman, K. L., Der, C. J. and Sondek, J. (2005). GEF means go: turning on RHO  
903 GTPases with guanine nucleotide-exchange factors. *Nat. Rev. Mol. Cell Biol.*  
904 6(2), 167–180.
- 905 Salazar, M. A., Kwiatkowski, A. V., Pellegrini, L., Cestra, G., Butler, M. H., Rossman,  
906 M. H., Serna, D. M., Sondek, J., Gertler, F. B. and de Camilli, P. (2003). Tuba, a  
907 novel protein containing bin/amphiphysin/Rvs and Dbl homology domains,  
908 links dynamin to regulation of the actin cytoskeleton. *J. Biol. Chem.* 278(49),  
909 49031–49043.
- 910 Sambrook, J., Fritsch, E. F. and Maniatis, T. (1989). *Molecular Cloning: A*  
911 *Laboratory Manual*, Cold Spring Laboratory Press, New York.
- 912 Schorey, C. D., D’Souza-Schorey, C., Boshans, R. L., McDonough, M., Stahl, P. D. and  
913 Van Aelst, L. (1997). A role for POR1, a Rac1-interacting protein, in  
914 ARF6-mediated cytoskeletal rearrangements. *EMBO J.* 16(17), 5445–5454.
- 915 Seshan, A., Bardin, A. J. and Amon, A. (2002). Control of Lte1 localization by cell  
916 polarity determinants and Cdc14. *Curr. Biol.* 12(24), 2098–2110.
- 917 Takei, K., Slpnev, V. I., Haucke, V. and de Camilli, P. (1999). Functional

- 918 partnership between amphiphysin and dynamin in clathrin-mediated  
919 endocytosis. *Nature Cell Biol.* 1(1), 33–39.
- 920 Tang, R. J., Breger, J., Idnurm, A., Gerik, K. J., Lodge, J. K., Heitman, J., Calderwood  
921 S. B. and Mylonakis, E. (2005). *Cryptococcus neoformans* gene involved in  
922 mammalian pathogenesis identified by a *Caenorhabditis elegans* progeny-  
923 based approach. *Infect. Immun.* 73(12), 8219–8225.
- 924  
925 Tarricone, C., Xiao, B., Justin, N., Walkier, P. A., Rittinger, K., Gamblin, S. J. and  
926 Smerdon, S. J. (2001). The structural basis of Arfaptin-mediated cross-talk  
927 between Rac and Arf signalling pathways. *Nature.* 411(6834), 215–219.
- 928 Van Aelst, L., Joneson, T. and Bar-Sagi, D. (1996). Identification of a novel Rac1-  
929 interacting protein involved in membrane ruffling. *EMBO J.* 15(15), 3778–  
930 3786.
- 931 Vanittanakom, N., Cooper, C. R., Fisher, M. C. and Sirisanthana, T. (2006).  
932 *Penicillium marneffei* infection and recent advances in the epidemiology and  
933 molecular biology aspects. *Clin. Microbiol. Rev.* 19(1), 95–110.
- 934 Verstrepen, K. J., Jansen, A., Lewitter, F. and Fink G. R. (2005). Intragenic tandem  
935 repeats generate functional variability. *Nature Genet.* 37(9), 986–990.
- 936 Verstrepen, K. J., Reynolds, T. B. and Fink, G. R. (2004). Origins of variation in the  
937 fungal cell surface. *Nature Rev Microbiol.*, 2(7), 533–540.
- 938 Webster, R. H. and Sil, A. (2008). Conserved factors Ryp2 and Ryp3 control cell  
939 morphology and infectious spore formation in the fungal pathogen  
940 *Histoplasma capsulatum*. *Proc. Natl. Acad. Sci. USA.* 105(38), 14573–14578.
- 941 Wendland, J. and Philippsen, P. (2001). Cell polarity and hyphal morphogenesis  
942 are controlled by multiple Rho-protein modules in the filamentous  
943 ascomycete *Ashbya gossypii*. *Genet.* 157(2), 601–610.
- 944 Yang, E., Wang, G., Woo, P. C. Y., Lau, S. K. P., Chow, W.-N., Chong, K. T. K., Tse, H.,  
945 Kao, R. Y., Chan, C. M., Che, X., Yuen, K. Y. and Cai, J. J. (2013). Unraveling the  
946 molecular basis of temperature-dependent genetic regulation in *Penicillium*  
947 *marneffei*. *Eukaryot Cell.* 12(9), 1214–1224.
- 948 Yoshida, S., Ichihashi, R. and Toh-e, A. (2003). Ras recruits mitotic exit regulator  
949 Lte1 to the bud cortex in budding yeast. *J. Cell Biol.* 161(5), 889–897.
- 950 Zhang, C., Luo, Z., He, D., Su, L., Yin, H., Wang, G., Liu, H., Rensing, C. and Wang, Z.  
951 (2018). FgBud3, a Rho4-interacting guanine nucleotide exchange factor, is  
952 involved in polarity growth, cell division and pathogenicity of *Fusarium*  
953 *graminearum*. *Front. Microbiol.* 9, 131.
- 954 Zimmerberg, J. and McLaughlin, S. (2004). Membrane curvature: how BAR  
955 domains bend bilayers. *Curr Biol.* 14(6), R250–R252.
- 956

957 **Figure legends**

958 **Figure 1. Relatedness of *T. marneffei* MsgA and other GEF-like proteins in**  
959 **fungi.**

960 (A) Bootstrapped relatedness tree of predicted Rho guanyl nucleotide exchange  
961 factor (GEF) proteins from a selection of dimorphic and monomorphic fungi.  
962 Black arrow indicates *T. marneffei* MsgA protein. The tree was generated using  
963 the maximum likelihood method based on JTT matrix model in CLUSTALW on  
964 MEGA7. Protein sequences are from *Saccharomyces cerevisiae* (Sc), *Candida*  
965 *albicans* (Ca), *Aspergillus nidulans* (AN), *Aspergillus fumigatus* (Afu), *Histoplasma*  
966 *capsulatum* (HCBG), *Coccidioides immitis* (CIMG), *Paracoccidioides brasiliensis*  
967 (PAAG), *Talaromyces stipitatus* (Ts) and *Talaromyces marneffei* (Tm). A  
968 previously characterised, archetypal member denotes each clade of Rho GEFs  
969 where possible: CDC24-like (CtlA), Bud3-like (BudC), RgfF, MsgA, TUS1-like  
970 (TusA) and ROM1/ROM2-like (RomB). MsgA belongs to a distinct class of Rho  
971 guanyl nucleotide exchange factor (GEF) proteins. (B) Expression of *T. marneffei*  
972 Rho GEF encoding genes across several growth conditions. These conditions  
973 include 24 h growth inside J774 murine macrophages (J774 macrophage  
974 infection) and THP-1 human macrophages (THP-1 macrophage infection), 24 h  
975 growth in macrophage-free cell culture media (J774 macrophage medium and  
976 THP-1 macrophage medium), 4 days hyphal growth at 25°C (25°C *in vitro*) and  
977 yeast growth at 37°C (37°C *in vitro*) *in vitro*. RNA was extracted and quantified by  
978 RNAseq analysis. MsgA shows upregulated expression during growth inside J774  
979 macrophages while the *ctlA*, *budC*, *tusA* and *romB* genes show expression across  
980 all conditions. The *rgfF* gene shows little to no expression under the tested  
981 conditions. Error bars represent the standard error of the mean.

982

983 **Figure 2. Deletion of *msgA* leads to aberrant growth inside macrophages.**

984 (A) The wildtype and  $\Delta msgA$  strains were grown on BHI medium at 25°C for 5  
985 days and 37°C for 6 days, stained with calcofluor (CAL) and examined. Both  
986 strains show indistinguishable growth characteristics with respect to growth  
987 rate and morphology in the hyphal (25°C) and yeast (37°C) form. (B) LPS  
988 activated J774 murine macrophages were infected with conidia from the  
989 wildtype,  $\Delta msgA$  and complemented  $\Delta msgA msgA^+$  strains and examined

990 microscopically. At 24 h post infection wildtype *T. marneffe*i within J774  
991 macrophages produced numerous ovoid yeast cells that divided by fission. In  
992 contrast the  $\Delta msgA$  mutant produced aberrantly shaped filaments, in addition to  
993 yeast cells. The complemented strain ( $\Delta msgA msgA^+$ ) was indistinguishable from  
994 the wildtype. (C) The effects of deleting *msgA* on morphogenesis in macrophages  
995 were quantified at the 24 h post infection time point. The  $\Delta msgA$  mutant strain  
996 showed  $37.4 \pm 0.49\%$  septate filaments compared to the wildtype and  
997 complemented  $\Delta msgA msgA^+$  strains, which had  $0.6 \pm 0.02\%$  and  $2.5 \pm 0.6\%$   
998 respectively. Additionally, the  $\Delta msgA$  strain showed a reduction in the number of  
999 yeast cells during macrophage infection with  $55.8 \pm 1.85\%$  compared to  
1000  $81.8 \pm 1.89\%$  and  $86 \pm 0.56\%$  in the wildtype and  $\Delta msgA msgA^+$  strains  
1001 respectively. Error bars represent the standard error of the mean with t-test  
1002 values falling in the following range  $** \leq 0.05$ . Images were captured using  
1003 differential interference contrast (DIC) or with epifluorescence to observe  
1004 calcofluor stained fungal cell walls (CAL). Scale bars are 10  $\mu m$ .

1005

1006 **Figure 3. Yeast cell formation defects in the  $\Delta msgA$  strain are not resolved**  
1007 **with prolonged incubation in macrophages.**

1008 LPS activated J774 murine macrophages were infected with conidia from the  
1009 wildtype,  $\Delta msgA$  and complemented  $\Delta msgA msgA^+$  strains and examined  
1010 microscopically after prolonged incubation. (A) At 48 h post infection wildtype  
1011 (*msgA*<sup>+</sup>) *T. marneffe*i within J774 macrophages retain their ovoid morphology  
1012 producing numerous yeast cells that divided by fission. However the septate  
1013 filaments produced by the  $\Delta msgA$  mutant strain at 24h post infection continued  
1014 to grow, showing increased length, rather than breaking down to form short  
1015 ellipsoid yeast cells (B) The effect of deleting *msgA* on morphogenesis in  
1016 macrophages was quantified at the 48 h post infection time point. Wildtype yeast  
1017 cells showed an average length of  $3.9 \pm 0.12 \mu m$  compared to the  $\Delta msgA$  mutant  
1018 strain, which produced yeast cells of an average cells length of  $8.9 \pm 0.57 \mu m$ ,  
1019 approximately 2.3 times longer than wildtype. The complemented strain ( $\Delta msgA$   
1020 *msgA*<sup>+</sup>) produced yeast cells of  $4.1 \pm 0.50 \mu m$  in length and was comparable to  
1021 wildtype. Error bars represent standard error of the mean with t-test values  
1022 falling in the following range  $*** \leq 0.001$ .

1023

1024 **Figure 4. Induced overexpression of *msgA* produces aberrant hyphae at**  
1025 **25°C and yeast cells with intracellular morphology at 37°C *in vitro*.**

1026 The wildtype (*msgA*<sup>+</sup>), inducible ( $\Delta$ *msgA xylP(p)::msgA*) and deletion mutant  
1027 ( $\Delta$ *msgA*) allele strains were grown in liquid BHI medium supplemented with  
1028 either 1% glucose (Uninduced) or 1% xylose (Induced) for 5 days at 25°C (A) or  
1029 6 days 37°C (B). Under uninduced conditions the  $\Delta$ *msgA xylP(p)::msgA* strain is  
1030 indistinguishable from  $\Delta$ *msgA* at both temperatures. (A) On inducing medium at  
1031 25°C the  $\Delta$ *msgA xylP(p)::msgA* strain shows increased septation (single  
1032 arrowheads) and branching (double arrowheads) along the entire length of the  
1033 hyphae but all other morphological and growth characters were  
1034 indistinguishable amongst the strains. (B) On inducing medium at 37°C the  
1035  $\Delta$ *msgA xylP(p)::msgA* strain produced yeast cells that are rounder and greatly  
1036 reduced in length compared to the  $\Delta$ *msgA* (single arrowheads). These yeast cells  
1037 were dividing by fission and resembled yeast cells produced during growth  
1038 inside macrophages. (C) Continuous induction over six days of growth of the  
1039  $\Delta$ *msgA xylP(p)::msgA* strain produces yeast cells that have polarity defects at  
1040 division and (D) a proportion of yeast cells appear to be dividing by budding  
1041 (white triangle). Images were captured using differential interference contrast  
1042 (DIC) or with epifluorescence to observe calcofluor stained fungal cell walls  
1043 (CAL). Scale bars are 10  $\mu$ m.

1044

1045 **Figure 5: MsgA localisation during growth inside J774 murine macrophages**

1046 LPS activated J774 murine macrophages were infected with a strain expressing  
1047 the *msgA::mCherry* fusion gene and incubated for 24 h. Cells were fixed and the  
1048 MsgA-mCherry fusion (MsgA) detected using an anti-mCherry rat monoclonal  
1049 (3F10) primary and an anti-rat ALEXA488 goat secondary antibody. Yeast cells  
1050 were also stained with calcofluor (CAL) to highlight the fungal cell wall. The  
1051 MsgA and CAL panels were also merged (Merge) to assess relative localisation  
1052 (A). MsgA was only evident in actively growing yeast cells and not in  
1053 ungerminated conidia (solid arrowhead) (B). In yeast cells MsgA is localised to  
1054 the cell membrane, immediately adjacent to the cell wall, and shows punctate  
1055 localisation in the cell membrane periphery, as well as both within the cytoplasm



1056 (D-E). Localization is not evident either at nascent septation sites prior to (B), or  
1057 immediately after (C)(single arrowheads), cell wall deposition. Instead it appears  
1058 in a region immediately adjacent to septation sites during cell separation (D-E)  
1059 (double arrowheads). Images were captured using differential interference  
1060 contrast (DIC) or with epifluorescence to observe calcofluor and ALEXA488  
1061 stained fungal features. Scale bars are 10  $\mu\text{m}$ .

1062

1063 **Figure 6: The BAR domain of *msgA* contributes to morphology during**  
1064 **growth inside macrophages.**

1065 (A) LPS activated murine macrophages infected with conidia of either the  
1066 wildtype (*msgA*<sup>+</sup>),  $\Delta\textit{msgA}$ ,  $\Delta\textit{msgA msgA}^{\Delta\textit{BAR}}$  or  $\Delta\textit{msgA msgA}^{\Delta\textit{DH}}$  strain. After 24 h  
1067 cells were fixed, stained with calcofluor (CAL) and examined microscopically.  
1068 Numerous small ellipsoid yeast cells dividing by fission were observed in  
1069 macrophages infected with the wildtype and  $\Delta\textit{msgA msgA}^{\Delta\textit{DH}}$  strains. In contrast  
1070 macrophages infected with  $\Delta\textit{msgA}$  and  $\Delta\textit{msgA msgA}^{\Delta\textit{BAR}}$  strains contained  
1071 septate filaments and elongated yeast-like cells. (B). The effects of the *msgA*  
1072 alleles on morphogenesis in macrophages were quantified at the 24 h post  
1073 infection time point. The  $\Delta\textit{msgA msgA}^{\Delta\textit{BAR}}$  mutant strain shows  $39.1\pm 0.6\%$  more  
1074 filaments and  $22.7\%\pm 0.5$  fewer yeast cells compared to wildtype. These numbers  
1075 are equivalent to those for the  $\Delta\textit{msgA}$  strain. In contrast the  $\Delta\textit{msgA msgA}^{\Delta\textit{DH}}$   
1076 strain was comparable to the wildtype and complemented  $\Delta\textit{msgA}$  strain. Error  
1077 bars represented SEM with t-test values falling in the following range \*\*  $\leq 0.05$   
1078 and \*\*\*  $\leq 0.001$ . Images were captured using differential interference contrast  
1079 (DIC) or with epifluorescence to observe calcofluor stained fungal cell walls  
1080 (CAL). Scale bars are 10 $\mu\text{m}$ .

1081

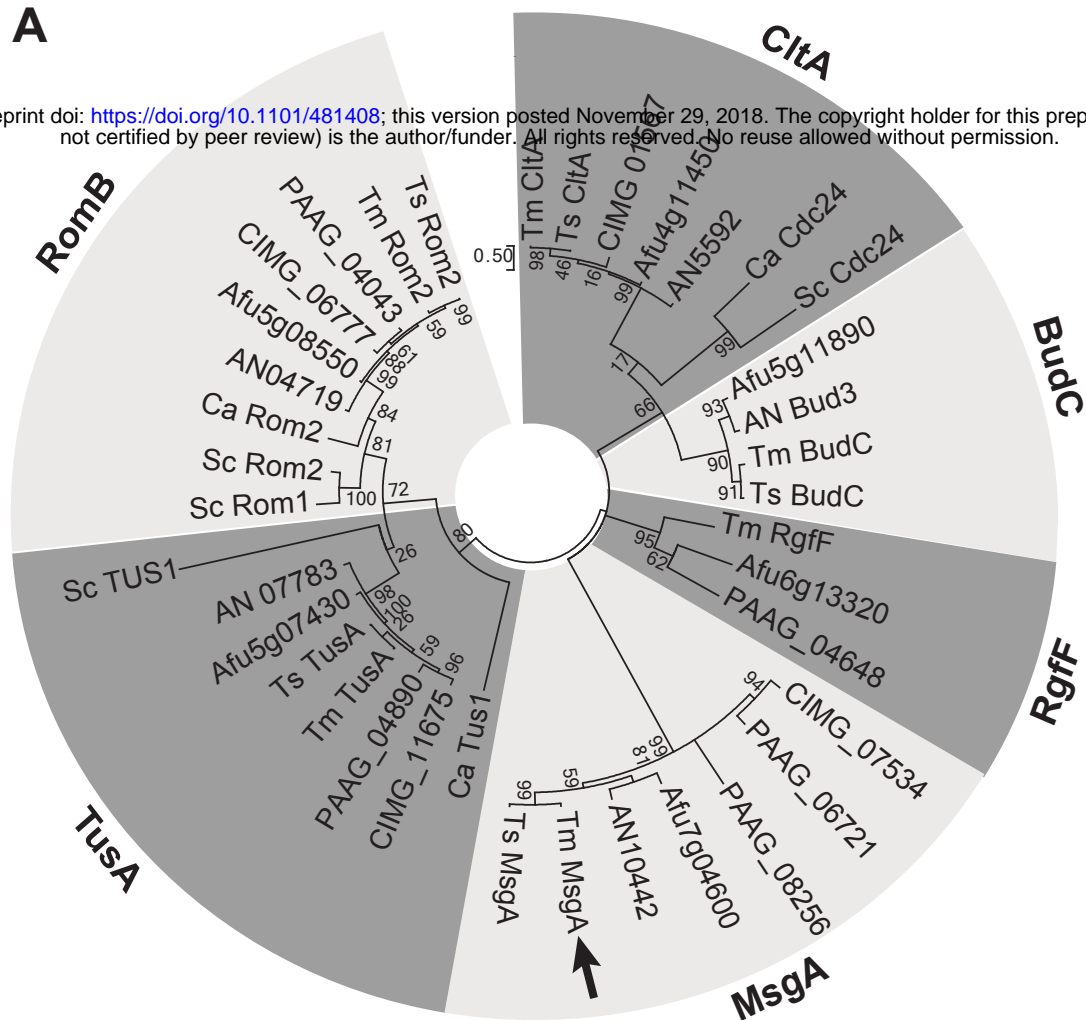
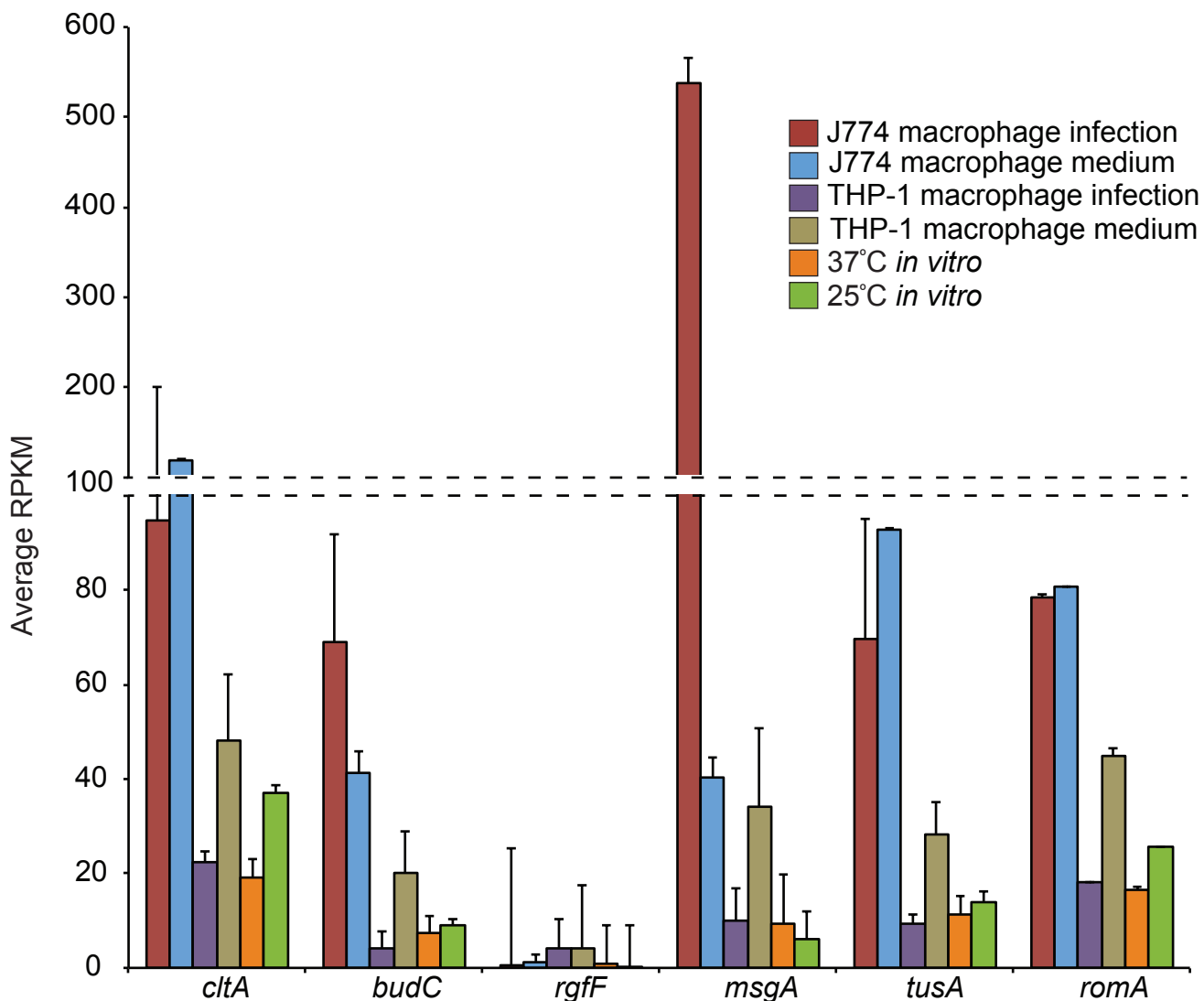
1082 **Figure 7: The BAR domain is necessary for the localisation of MsgA during**  
1083 **growth inside macrophages**

1084 LPS activated murine macrophages infected with conidia from the wildtype  
1085 (*msgA::mCherry*), *msgA* <sup>$\Delta\textit{BAR}$</sup> ::*mCherry* or *msgA* <sup>$\Delta\textit{DH}$</sup> ::*mCherry* strain. After 24 h cells  
1086 were fixed and the MsgA-mCherry fusion (MsgA) alleles was detected using an  
1087 anti-mCherry rat monoclonal (3F10) primary and an anti-rat ALEXA488 goat  
1088 secondary antibody. Yeast cells were also stained with calcofluor (CAL) to

1089 highlight the fungal cell wall. Both MsgA and CAL panels were overlaid to  
1090 indicate overlapping localisation (Merge). The wildtype *msgA::mCherry* gene  
1091 product showed clear punctate cell membrane localisation with puncta also  
1092 within the cytoplasm (*msgA::mCherry* panel). This pattern of localisation was  
1093 also evident for the *msgA<sup>ΔDH</sup>::mCherry* gene product (*msgA<sup>ΔDH</sup>::mCherry* panel).  
1094 However the *msgA<sup>ΔBAR</sup>::mCherry* gene product has lost its punctate pattern of  
1095 localisation and appears uniformly within the cytoplasm. Additionally the  
1096 *msgA<sup>ΔBAR</sup>::mCherry* gene product was mislocalized to the cell wall co-staining  
1097 with calcofluor throughout the cell periphery (*msgA<sup>ΔBAR</sup>::mCherry* panel). As with  
1098 the wildtype *msgA::mCherry* strain (Figure 5) the *msgA<sup>ΔDH</sup>::mCherry* gene product  
1099 localized to the region immediately adjacent division septum during cell  
1100 separation (double arrowheads). In contrast the *msgA<sup>ΔBAR</sup>::mCherry* gene product  
1101 was mislocalized to the cell wall, co-staining with calcofluor, during cell  
1102 separation (solid arrowhead) but not at nascent septation sites prior to (single  
1103 arrowheads) cell wall deposition. Images were captured using differential  
1104 interference contrast (DIC) or with epifluorescence to observe calcofluor (CAL)  
1105 and ALEXA488 fluorophores. Scale bars are 10 μm.

**A**

bioRxiv preprint doi: <https://doi.org/10.1101/481408>; this version posted November 29, 2018. The copyright holder for this preprint (which was not certified by peer review) is the author/funder. All rights reserved. No reuse allowed without permission.

**B**

**A**

bioRxiv preprint doi: <https://doi.org/10.1101/481408>; this version posted November 29, 2018. The copyright holder for this preprint (which was not certified by peer review) is the author/funder. All rights reserved. No reuse allowed without permission.

25°C

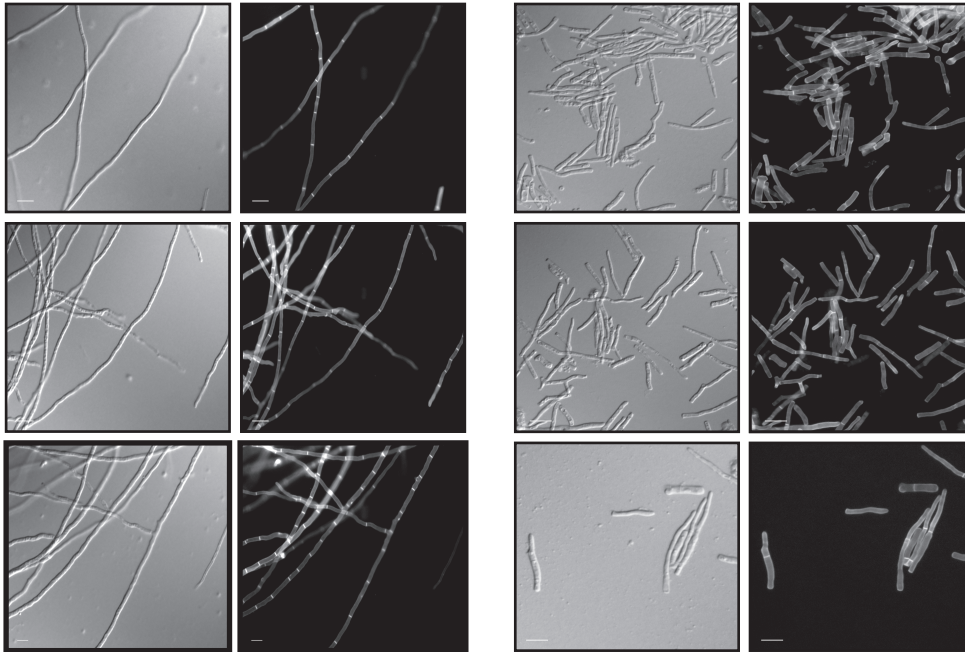
37°C

DIC

CAL

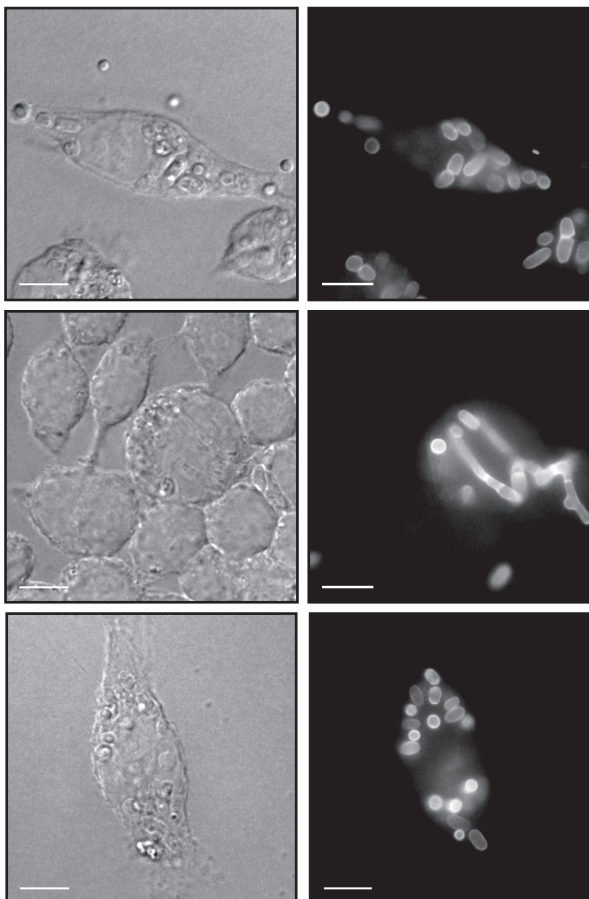
DIC

CAL

*msgA*<sup>+</sup> $\Delta$ *msgA* $\Delta$ *msgA msgA*<sup>+</sup>**B**

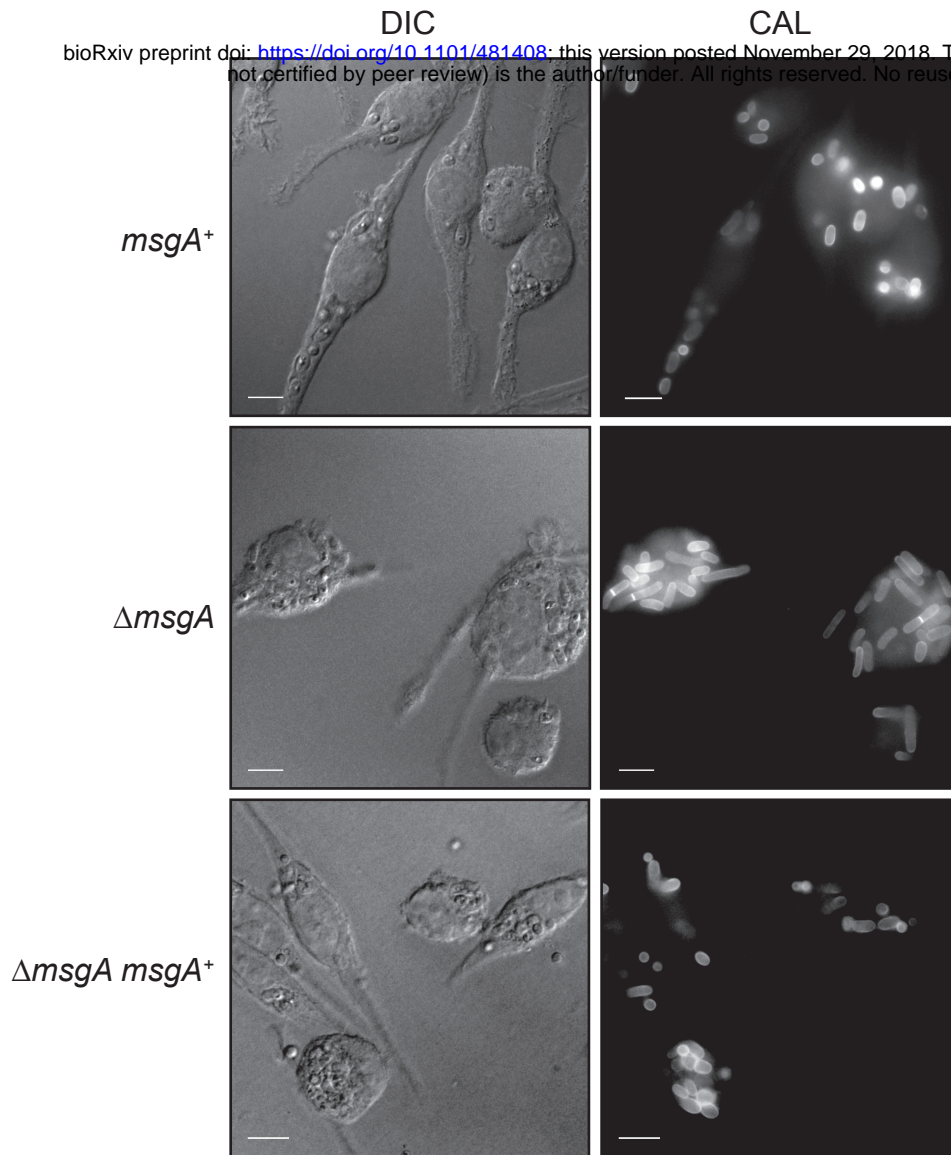
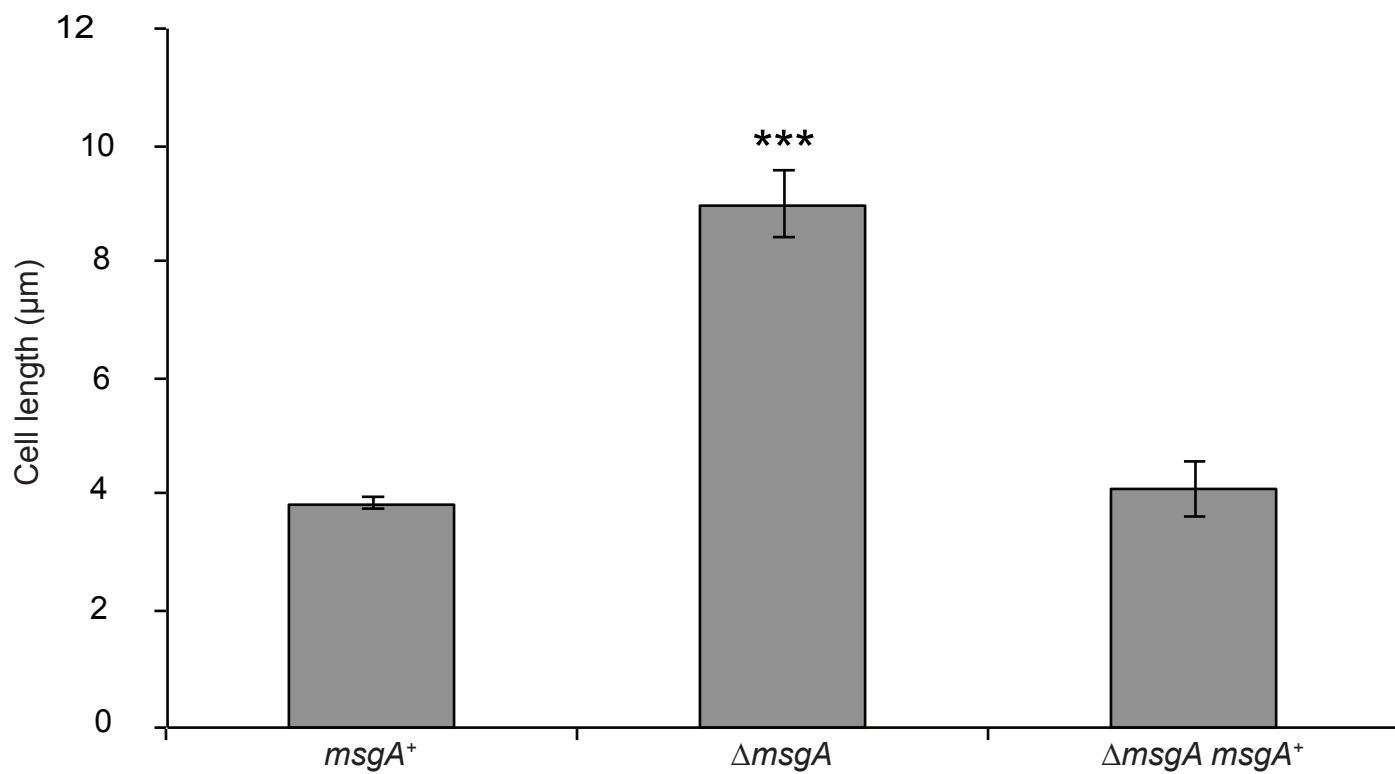
DIC

CAL

*msgA*<sup>+</sup> $\Delta$ *msgA* $\Delta$ *msgA msgA*<sup>+</sup>

**A**

bioRxiv preprint doi: <https://doi.org/10.1101/481408>; this version posted November 29, 2018. The copyright holder for this preprint (which was not certified by peer review) is the author/funder. All rights reserved. No reuse allowed without permission.

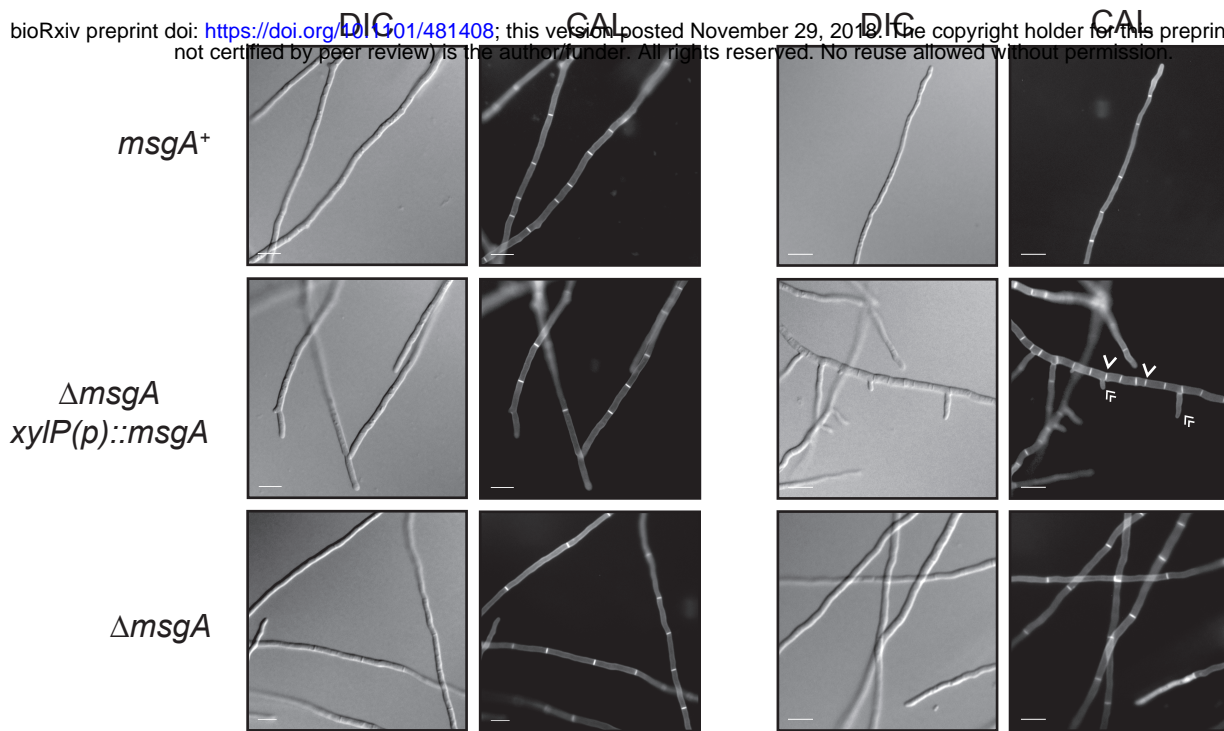
**B**

**A**

Uninduced

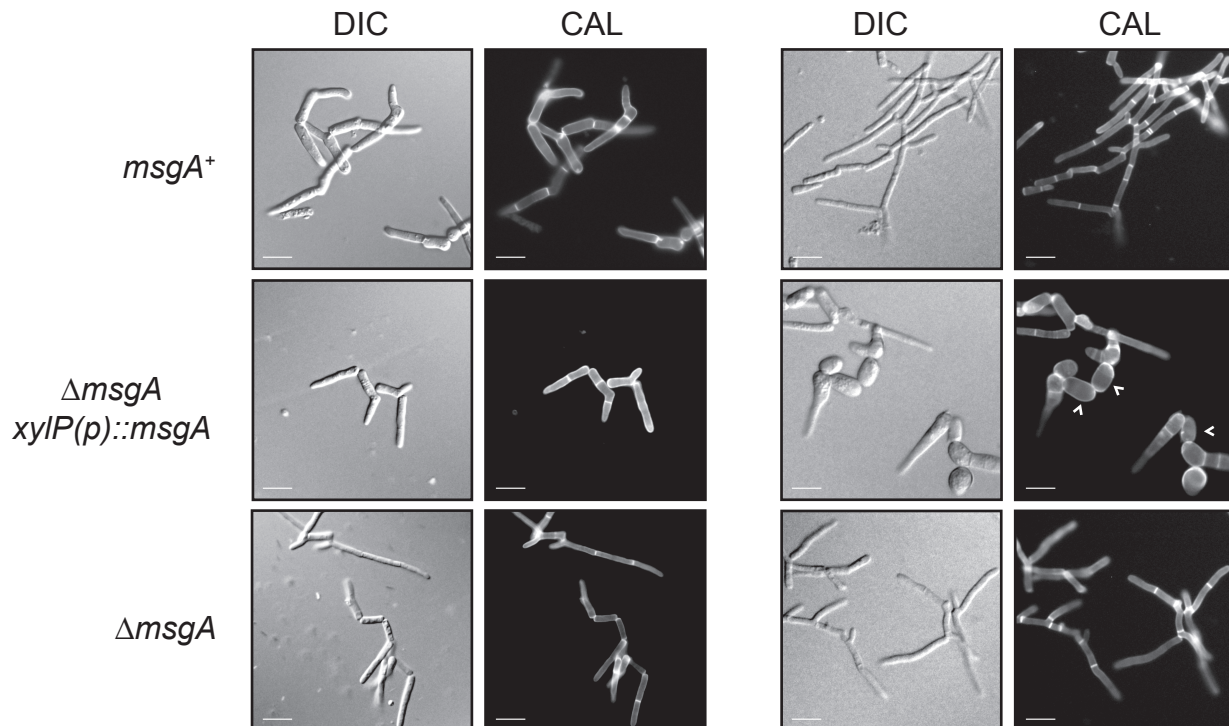
Induced

bioRxiv preprint doi: <https://doi.org/10.1101/481408>; this version posted November 29, 2019. The copyright holder for this preprint (which was not certified by peer review) is the author/funder. All rights reserved. No reuse allowed without permission.

**B**

Uninduced

Induced

**C**

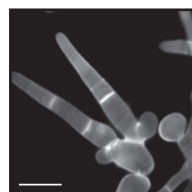
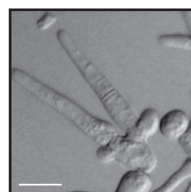
DIC

CAL

$\Delta$ *msgA*  
*xyIP(p)::msgA*



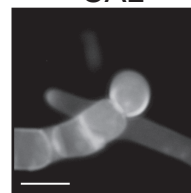
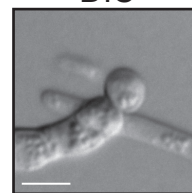
$\Delta$ *msgA*  
*xyIP(p)::msgA*

**D**

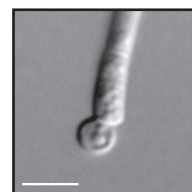
DIC

CAL

$\Delta$ *msgA*  
*xyIP(p)::msgA*

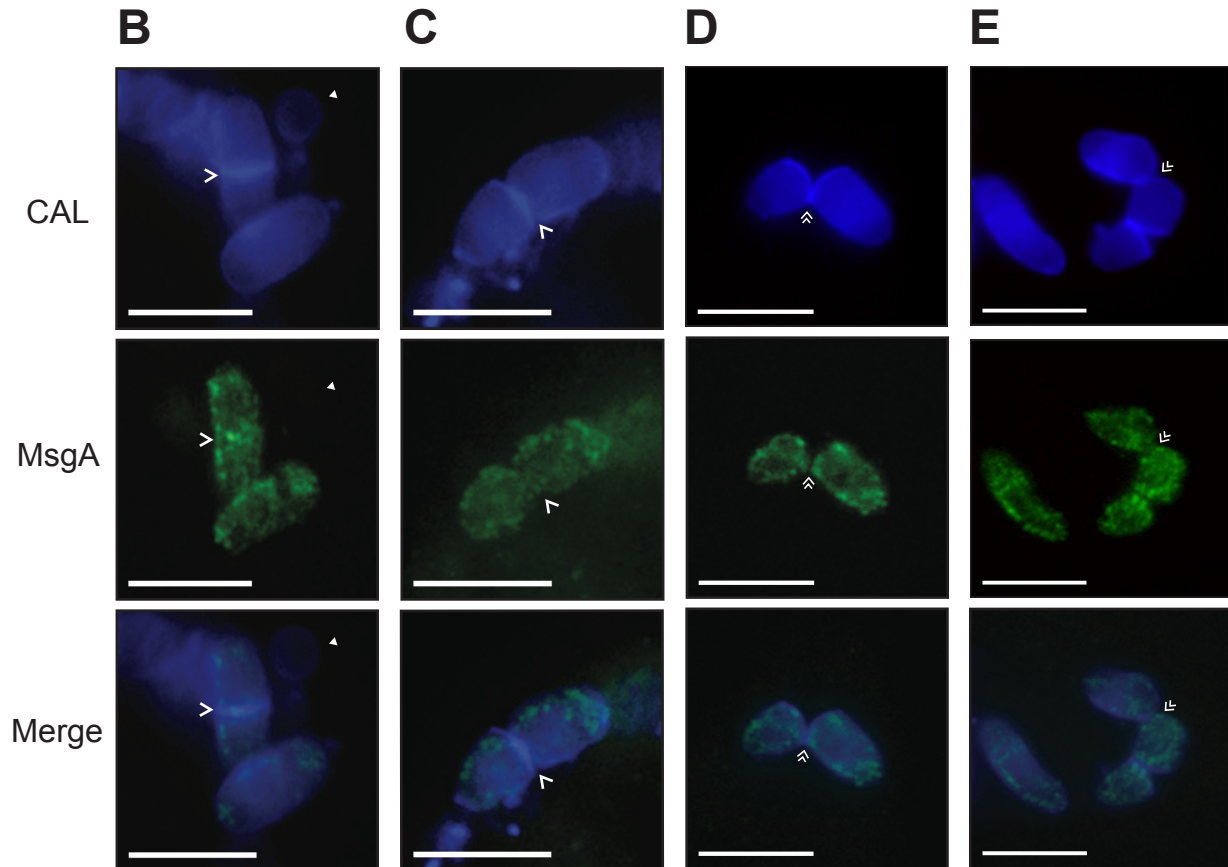
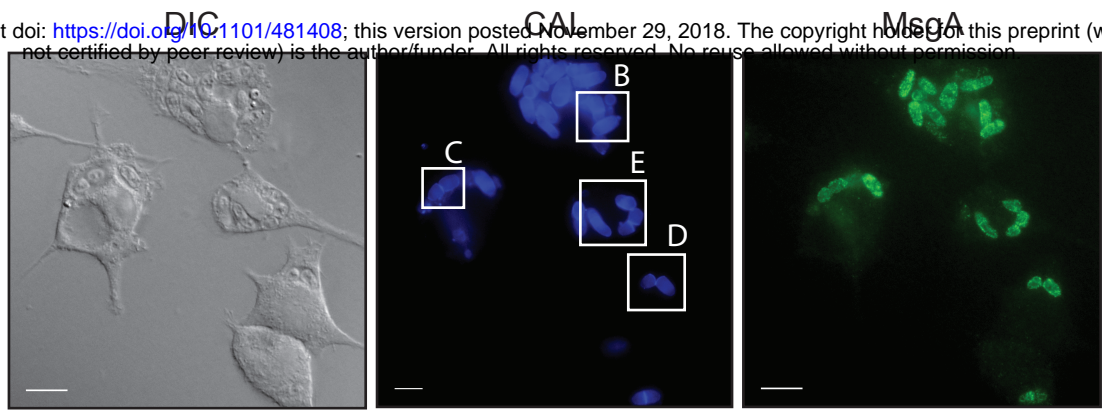


$\Delta$ *msgA*  
*xyIP(p)::msgA*



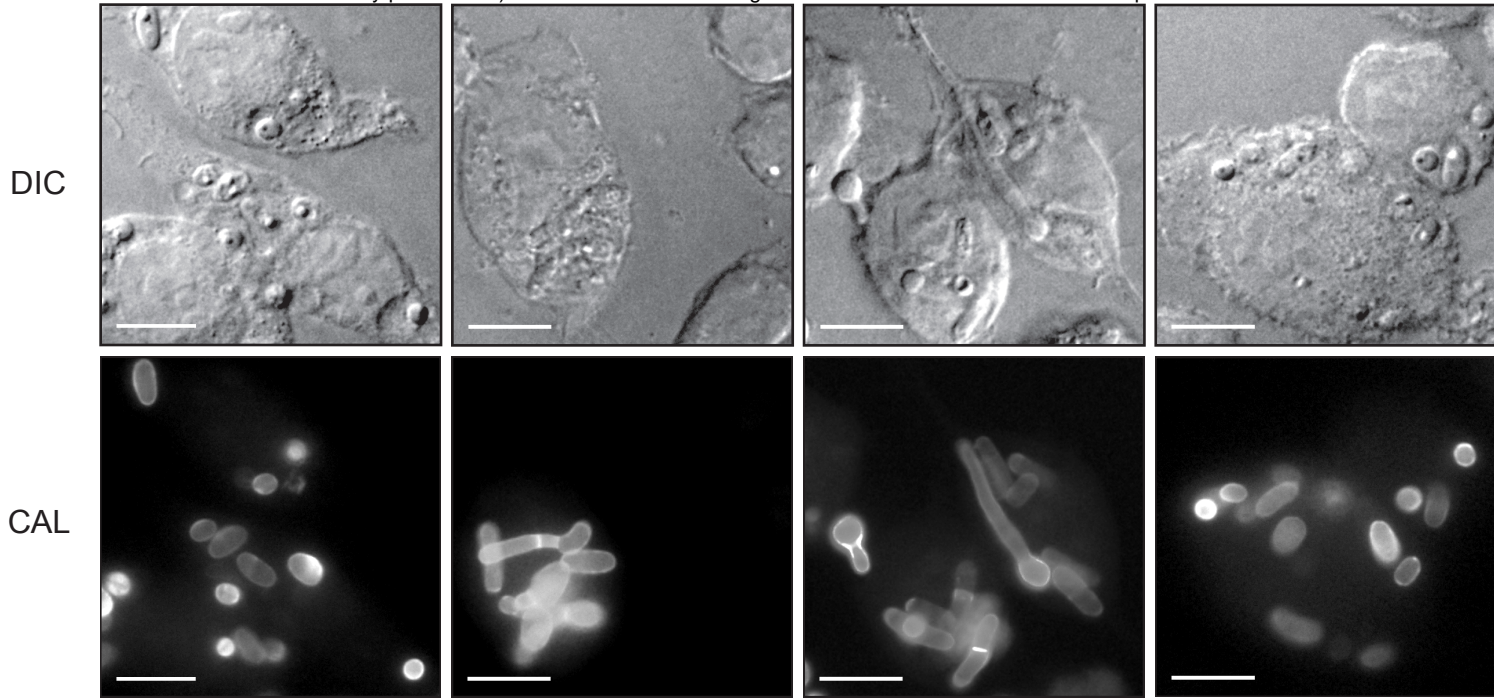
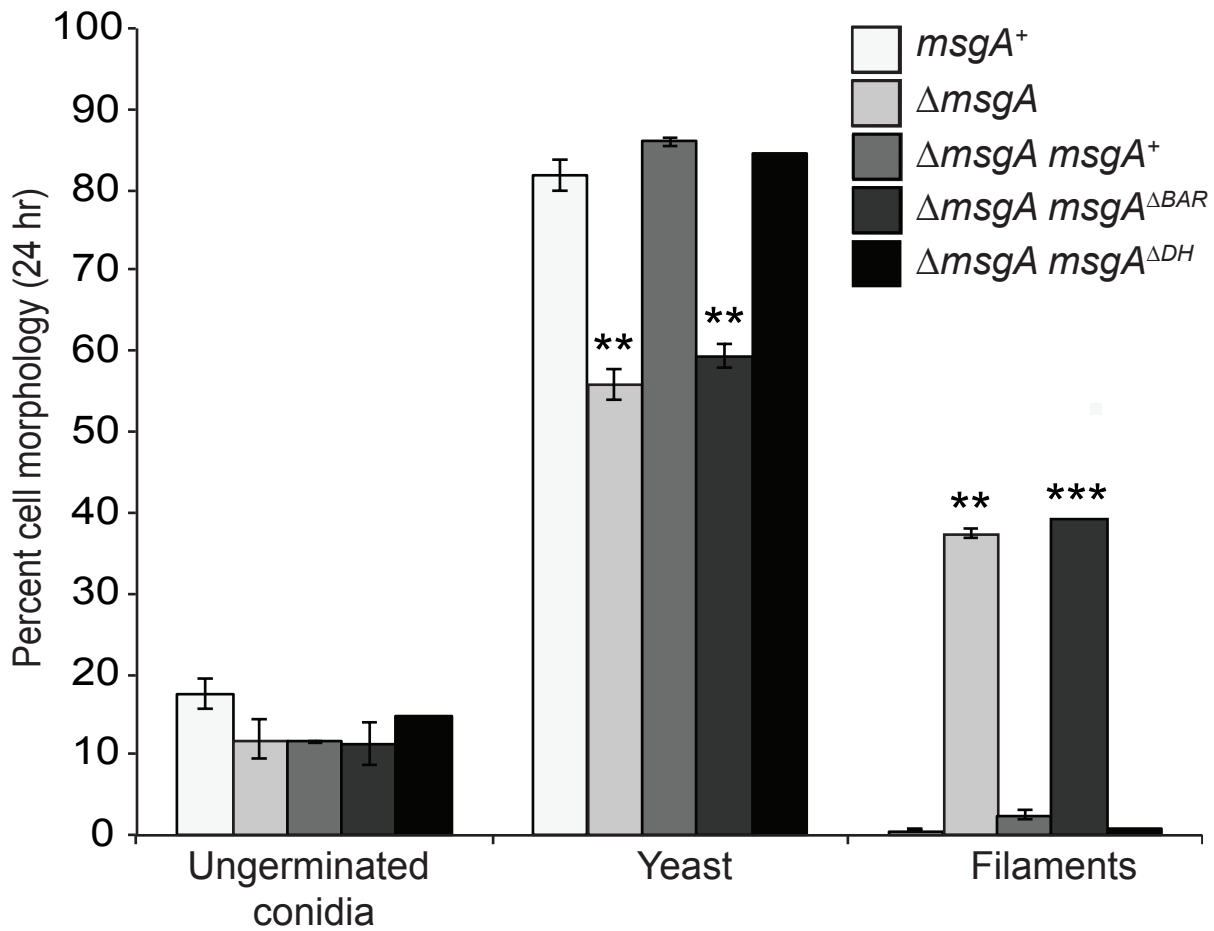
**A**

bioRxiv preprint doi: <https://doi.org/10.1101/481408>; this version posted November 29, 2018. The copyright holder for this preprint (which was not certified by peer review) is the author/funder. All rights reserved. No reuse allowed without permission.



**A**

bioRxiv preprint doi: <https://doi.org/10.1101/481408>; this version posted November 29, 2018. The copyright holder for this preprint (which was not certified by peer review) is the author/funder. All rights reserved. No reuse allowed without permission.

**B**



*msgA::mCherry*

*msgA<sup>ΔBAR</sup>::mCherry*

*msgA<sup>ΔDH</sup>::mCherry*

bioRxiv preprint doi: <https://doi.org/10.1101/461406>; this version posted November 29, 2018. The copyright holder for this preprint (which was not certified by peer review) is the author/funder. All rights reserved. No reuse allowed without permission.

